METHODS AND APPROACHES

A novel voltage-clamp/dye uptake assay reveals saturable transport of molecules through CALHM1 and connexin channels

Pablo S. Gaete[1], Mauricio A. Lillo[1], William López[1], Yu Liu[1], Wenjuan Jiang[2], Yun Luo[2], Andrew L. Harris[1], and Jorge E. Contreras[1]

Large-pore channels permeable to small molecules such as ATP, in addition to atomic ions, are emerging as important regulators in health and disease. Nonetheless, their mechanisms of molecular permeation and selectivity remain mostly unexplored. Combining fluorescence microscopy and electrophysiology, we developed a novel technique that allows kinetic analysis of molecular permeation through connexin and CALHM1 channels in *Xenopus* oocytes rendered translucent. Using this methodology, we found that (1) molecular flux through these channels saturates at low micromolar concentrations, (2) kinetic parameters of molecular transport are sensitive to modulators of channel gating, (3) molecular transport and ionic currents can be differentially affected by mutation and gating, and (4) N-terminal regions of these channels control transport kinetics and permselectivity. Our methodology allows analysis of how human disease–causing mutations affect kinetic properties and permselectivity of molecular signaling and enables the study of molecular mechanisms, including selectivity and saturability, of molecular transport in other large-pore channels.

Introduction

Large-pore channels are characterized by permeability to both atomic ions and small molecules. In vertebrates, examples of large-pore channels include those formed by calcium homeostasis modulator (CALHM), connexins, pannexins, and leucine-rich repeat–containing 8 (LRRC8). Although they have some properties in common, such as membrane topology, pharmacological profiles, and permeants, recent structural and functional evidence indicates that gating and selectivity mechanisms differ for each channel.

The CALHM family includes six members: CALHM1–6. CALHM1, the most studied isoform, is expressed mainly in the brain and has been associated with control of neuronal excitability and sensory perception (Dreses-Werringloer et al., 2008; Ma et al., 2012; Taruno et al., 2013). CALHM1 forms voltage-gated and Ca^{2+}-sensitive channels with a wide pore (estimated to be >14 Å in diameter in the narrowest zone of the conduction pathway) that allows the nonselective transport of Ca^{2+}, K^+, Na^+, monovalent anions, and small molecules such as ATP and fluorescent dyes (Siebert et al., 2013; Ma et al., 2016; Demura et al., 2020; Syrjanen et al., 2020).

Connexins are the proteins that compose gap junction channels (GJCs) in vertebrates. GJCs are formed by the docking of two connexin hemichannels, each provided by adjacent cells. When hemichannels are undocked, they provide an autocrine/paracrine signaling route by a gated pathway between the intracellular compartment and the extracellular milieu (Sáez et al., 2003). With 21 isoforms in humans, the connexin family represents the most diverse group of large-pore membrane channels. They are ubiquitously expressed in almost all human tissues. On the basis of structural data and permeability profiles, it is thought that the narrowest diameter of the pore of the hemichannels is ~12–15 Å (Harris, 2007; Maeda et al., 2009; Sáez and Leybaert, 2014; Myers et al., 2018). Thus, connexin hemichannels are known as conduits not only for atomic ions but also for small biological molecules such as ATP, inositol trisphosphate, cAMP, nitric oxide, glutamate, prostaglandins, and NAD^+ (Harris, 2007; Figueroa et al., 2013).

The opening of large-pore channels, including connexin hemichannels and CALHM1 channels, is commonly evaluated using conventional electrophysiological techniques and dye uptake/efflux assays, whose readouts are ionic currents and molecular permeability to fluorescent dyes, respectively. Nevertheless, recent evidence suggests that permeability to molecules cannot be extrapolated to atomic ion permeation and vice

[1]Department of Pharmacology, Physiology, and Neuroscience, New Jersey Medical School, Rutgers, The State University of New Jersey, Newark, NJ; [2]Department of Pharmaceutical Sciences, College of Pharmacy, Western University of Health Sciences, Pomona, CA.

Correspondence to Jorge E. Contreras: contrejo@njms.rutgers.edu.

versa. For example, the uptake of molecular dyes through connexin and pannexin channels has been reported at resting membrane potentials at which atomic ion currents through those channels are not detected (Contreras et al., 2003; Hansen et al., 2014a, 2014b; Nielsen et al., 2020). Furthermore, pharmacological blockade of connexins or pannexins has been shown to differentially affect atomic ion and molecular permeation (Nielsen et al., 2019, 2020). These data suggest that the mechanisms of transport for ions and molecules may be distinct.

The most common and simple experimental strategy to evaluate the activity of these channels is via uptake of small molecular fluorescent dyes such as ethidium, YO-PRO, propidium iodide, Lucifer yellow, and 4′,6-diamidino-2-phenylindole dilactate (DAPI; Orellana et al., 2011; Siebert et al., 2013; Hansen et al., 2014b; Sáez and Leybaert, 2014; Gaete et al., 2019; Lillo et al., 2019). However, this methodology often presents experimental disadvantages, such as low temporal resolution and uncontrolled membrane potentials. Lack of normalization due to the inherent variability of protein expression and the number of functional channels located at the plasma membrane makes this methodology only a qualitative tool, insufficient to provide a basis for biophysical analysis of molecular permeation. To more rigorously study the biophysical properties of permeation in large-pore channels, an integrated approach is needed that is capable of analyzing in the same preparation the kinetics of transport of molecules and atomic ions.

To address these issues, we developed a novel method that examines both ionic currents and permselectivity to fluorescent dyes simultaneously using translucent *Xenopus laevis* oocytes. By applying this technique, we found novel and exciting biophysical properties in both connexin hemichannels and CALHM1 channels. The method revealed saturation of molecular flux and allowed us to quantify kinetic parameters of molecular permeability (V_{max} and K_m) at controlled membrane potential conditions. This methodology will also permit quantitative exploration of permeation of ions and molecules in other wide-pore channels, including innexin, pannexin, and LRRC8 channels.

Materials and methods
Collection of oocytes
Oocytes were collected from female *Xenopus* according to the experimental protocol approved by the institutional animal care and use committee at Rutgers University and conforming to the National Institutes of Health Guide for the Care and Use of Laboratory Animals. Briefly, frogs were anesthetized by immersion in a 0.35% ethyl 3-aminobenzoate methanesulfonate (MS-222) solution adjusted to pH 7.0–7.5. Subsequently, one ovarian lobe was excised to collect the oocytes. Oocytes were defolliculated using an OR-2 solution (composition in mM: 82.5 NaCl, 2.5 KCl, 1 $MgCl_2$, and 5 HEPES, adjusted to pH 7.6) containing 0.3% collagenase type IA. Then, oocytes were stored at 16°C in an ND96 solution (composition in mM: 96 NaCl, 2 KCl, 1 $MgCl_2$, 1.8 $CaCl_2$, and 5 HEPES, adjusted to pH 7.4) supplemented with 50 µg/ml streptomycin plus 50 U/ml penicillin.

Molecular biology and channel expression
cDNA for human (h) CALHM1, hCx26, and hCx30 were synthesized by Epoch Life Science. cDNAs were amplified, and PCR fragments were subcloned into pGEM-HA vector (Promega) for expression in *Xenopus* oocytes. The cDNAs were transcribed in vitro to cRNAs using the T7 Message Machine Kit (Ambion). Single mutations in Cx26 and Cx30 were produced using the QuickChange II Site-Directed Mutagenesis Kit (Agilent Technologies).

Healthy, mature, nonfertilized oocytes (stages IV and V) were individually microinjected with cRNA for CALHM1, Cx26, Cx26[N14K], Cx30, or Cx30[G11R] using the Nanoliter 2010 injection system (World Precision Instruments). Then, oocytes were stored separately in ND96 solution at 16°C. After 1–2 d, oocytes were used for electrophysiology experiments, Western blotting, or underwent a protocol to render the animal pole translucent (see below). The amount of injected cRNA for electrophysiology and dye uptake experiments ranged from 10 ng to 50 ng per oocyte. For those experiments in which electrophysiological properties were measured at zero Ca^{2+}, oocytes were injected with 1–5 ng per oocyte. For biotinylation experiments, 10 ng Cx30 or 10 ng Cx30[G11R] was injected into each oocyte.

Xenopus oocytes express endogenous Cx38, which could interfere with the analysis and interpretation of the acquired data (Ebihara, 1996). Therefore, to reduce the expression levels of Cx38, all the oocytes (including control oocytes not expressing exogenous proteins) were injected with an antisense oligonucleotide (0.5 µg/µl), using a sequence described previously (Ebihara, 1996). The effectiveness of this antisense was confirmed by functional assays (Fig. S1).

Preparation of translucent oocytes
Detection of fluorescence in intact *Xenopus* oocytes is challenging because of their high and variable intrinsic autofluorescence and the high content of pigments and yolk granules that make difficult the detection of a fluorescent signal from the cytoplasm (Dumont, 1972; Lee and Bezanilla, 2019). To detect fluorescence emitted from the intracellular compartment, we rendered oocytes translucent. To achieve this, we optimized a centrifugation procedure previously reported by Iwao et al. (1997). Briefly, Eppendorf tubes containing 350 µl of 45% Ficoll PM 400 were gently filled with 350 µl of ND96 solution with special care taken not to mix the two solutions. Then, oocytes were individually immersed into the tubes so that the oocytes were retained at the interface between Ficoll and the ND96 solutions. In this interface, the animal pole of the oocyte faces up. The tubes were then centrifuged for 30 min at 1,700 *g* and 4°C. After centrifugation, oocytes were carefully collected and rinsed with ND96 to remove Ficoll. Centrifuged oocytes were stored at 16°C in ND96 solution for ≥30 min before microinjection of DNA and/or DAPI (see below). In one experimental series, the centrifugation force applied ranged between 100 and 3,000 *g* to characterize the procedure.

DNA microinjection
The most common dyes used to study molecular permeability through large-pore channels, such as ethidium and YO-PRO, require intercalation with helical polynucleotides to strongly

increase their fluorescent emission. To enhance the sensitivity of our technique and to provide a vast excess of binding sites for the polynucleotide-dependent fluorescent molecules, centrifuged oocytes were microinjected with ~50 nl of a solution containing DNA extracted from salmon testes (0.5 mg/ml) and DAPI (100 µM). In one experimental series, oocytes were injected with DNA alone, DAPI alone, or water as a control. Microinjection was performed using the Nanoliter 2010 injection system (World Precision Instruments). The pipette was placed in the line that separates the animal pole from the vegetal pole, and microinjections always were oriented toward the translucent zone (animal pole). DAPI was coinjected to visualize the location of the DNA where fluorescence would be emitted after binding of permeable molecules tested; in this case, ethidium or YO-PRO. Importantly, at the concentrations used, DAPI did not compromise the sensitivity to other fluorescent dyes, such as ethidium (Fig. S2). After microinjection, oocytes were stored in ND96 solution at 16°C. Resting membrane potential became less negative immediately after centrifugation but soon recovered. Therefore, we kept the oocytes in ND96 at 16°C for ≥2 h before conducting any experiment with translucent oocytes.

Fluorescence microscopy imaging
Oocytes were transferred to a chamber containing Ringer solution (composition in mM: 115 NaCl, 2 KCl, 1.8 CaCl$_2$, and 5 HEPES, adjusted to pH 7.4) and placed on the stage of an inverted epifluorescence microscope (Zeiss Axiovert 200M). Images were acquired using a Zeiss AxioCam MRm camera and the AxioVision 4.8 software (Carl Zeiss).

Electrophysiology
Whole-cell recordings and membrane potential measurements were performed using the two-electrode voltage-clamp technique (TEVC). For TEVC, two pulled borosilicate glass micropipettes were filled with 3 M KCl, obtaining resistances ranging from 0.2 to 2 MΩ. Electrodes for voltage recordings and current injection were mounted on separate micromanipulators (Burleigh PCS-5000) on the stage of a Nikon Eclipse Ti microscope. The electrical signal was amplified using an oocyte clamp amplifier (OC-725C; Warner Instrument Corp.) and digitized by a data acquisition system (Digidata 1440A; Molecular Devices). Data were sampled at 2 kHz, acquired at room temperature (20–22°C), and analyzed using the pClamp 10 software (Molecular Devices).

Dye uptake
Oocytes were individually transferred to a perfusion chamber containing Ringer solution and placed on the stage of an inverted epifluorescence microscope (Nikon Eclipse Ti). The chamber was adapted to include a small hole (diameter, ~1 mm), designed to keep the oocyte immobile in the center of the microscope platform. A transparent coverslip at the bottom of the hole faced the objective of the microscope. The oocyte was positioned in the central hole with the vegetal pole facing up and the translucent side (the animal pole) facing down toward the objective of the inverted microscope. Then, two electrodes were gently placed into the vegetal pole to perform TEVC in the same oocyte in which dye uptake was evaluated (i.e., the TEVC/dye uptake

assay; Fig. 1 E). The uptake of 0.1–25 µM YO-PRO (375 D; charge, +2) or 0.1–50 µM ethidium (314 D; charge, +1) was assessed at resting membrane potential (unless otherwise stated) ≥10 min after the oocyte was impaled (to allow recovery from the microelectrode impalement).

Dye uptake was recorded in real time using a photomultiplier tube (PMT1002; Thorlabs) connected to a data acquisition system (Digidata 1440A; Molecular Devices). Data were acquired at 2 kHz and analyzed using the pClamp 10 software (Molecular Devices). The oocytes were incubated with the fluorescent dyes 10 min before the recording of the dye uptake.

The rates of dye uptake were obtained by subtracting background autofluorescence and calculating the slope of dye uptake recorded over 10 min. Dye uptake along the time course is expressed as arbitrary units (A.U.) and dye uptake rates are expressed as A.U./min. For experiments using ethidium, a gravity-dependent flow of 0.5 ml/min was used. For experiments performed with YO-PRO, no flow was used. All measurements were made at room temperature (20–22°C) in darkness.

Because extracellular divalent cations (such as Ca^{2+}) inhibit CALHM1 and connexin hemichannels, dye uptake was evaluated using a divalent cation-free Ringer solution (composition in mM: 115 NaCl, 2 KCl, and 5 HEPES, adjusted to pH 7.4). This solution did not contain any chelating agents such as EDTA or EGTA, and it was likely to contain a negligible concentration of Ca^{2+}. The effect of extracellular Ca^{2+} (1 mM) on molecular permeation through CALHM1 was also evaluated.

For measurements under voltage-clamp conditions, we used oocytes expressing CALHM1 exposed to 1 mM Ca^{2+}. Dye uptake recordings started 3 min after the voltage was clamped and extended for 10 min for each voltage tested. Oocytes usually do not maintain steady currents after extended or repeated voltage clamping. For that reason, no more than two or three voltages were tested per oocyte.

In some experimental series, dye uptake was assessed in permeabilized oocytes. For this, centrifuged oocytes that did not express exogenous channels were incubated in ND96 solution containing 0.01% Triton X-100 for 30 s and subsequently washed with ND96 for 1 min. Then, oocytes were incubated with dyes dissolved in a divalent cation-free Ringer solution. Dye uptake in permeabilized oocytes was measured at resting membrane potential and at room temperature. To obtain representative images of dye uptake, some permeabilized oocytes were incubated for 3 min with 7.5 µM YO-PRO, 7.5 µM ethidium bromide, or vehicle alone (as a control for autofluorescence).

Analysis of the biophysical properties of exogenous channels expressed in *Xenopus* oocytes
To analyze the biophysical properties of CALHM1 and connexins, we analyzed the currents activated by voltage-step pulses from –80 mV to 0 mV in Ringer solution containing 1.8 mM Ca^{2+} (unless otherwise stated). Additionally, Ca^{2+} concentration–response curves were obtained by analyzing the magnitude of tail currents evoked by depolarizing pulses (–80 mV to 0 mV; duration, 40 s), as described previously by Lopez et al. (2013). The Ca^{2+} concentration–response relationship was fit to the Hill equation using Origin 9 software (OriginLab Corp.).
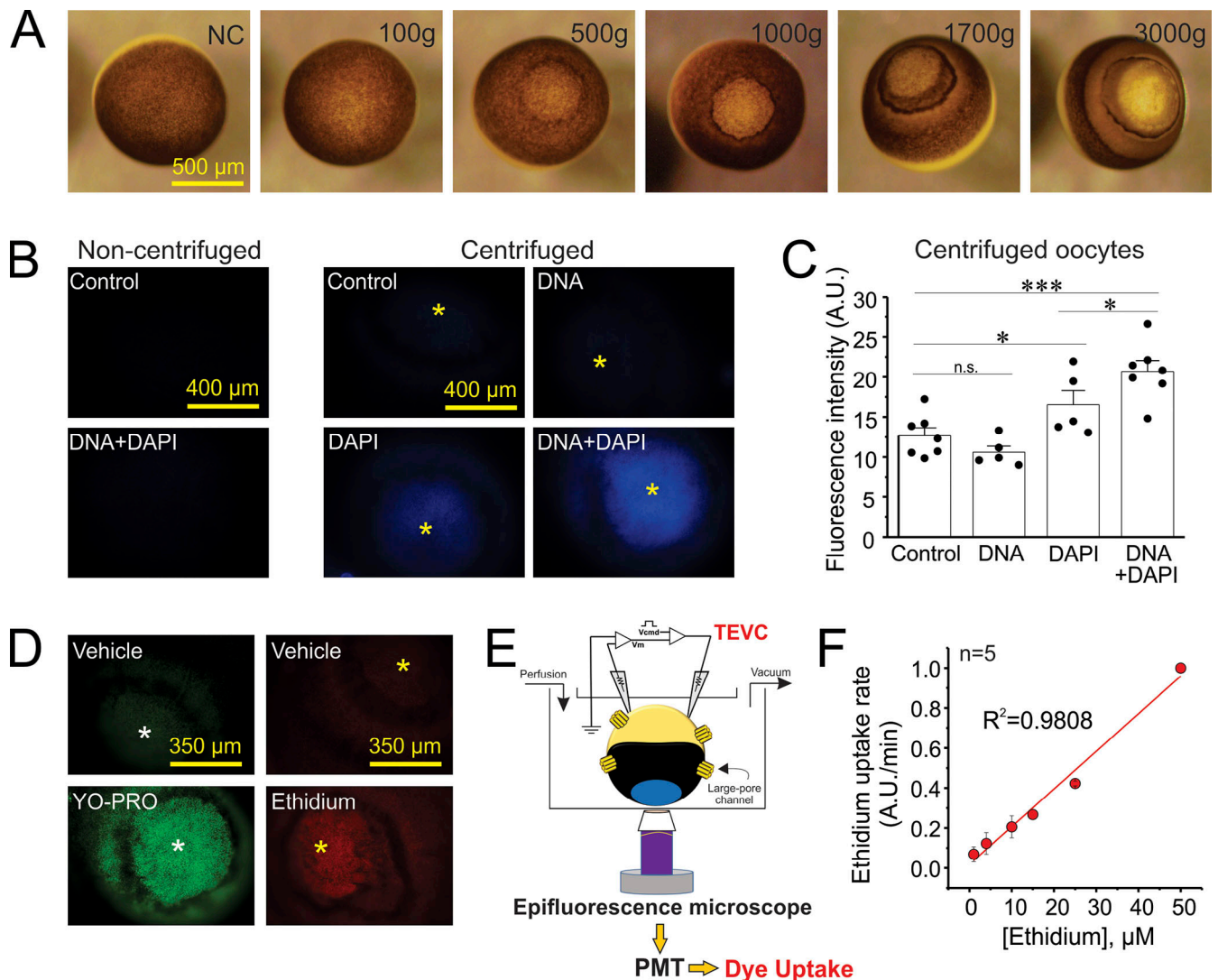
Figure 1. **A centrifugation procedure turns oocytes translucent and improves visualization of polynucleotide-dependent fluorescent dyes. (A)** Centrifugal force renders animal pole translucent. NC, noncentrifuged. **(B)** Representative fluorescent signal (excitation filter, 350 nm; emission filter, 460 nm) detected in noncentrifuged oocytes injected with DNA plus DAPI or water (as a control). The fluorescent signal detected in centrifuged oocytes is shown in the right panel. Asterisks indicate the translucent zone in the animal pole. **(C)** Quantification of the fluorescent signal in centrifuged oocytes shown in B. *, P < 0.05; ***, P < 0.001 by one-way ANOVA plus Newman-Keuls post hoc test; n.s., nonsignificant. Error bars are SEM. **(D)** Representative pictures of YO-PRO or ethidium uptake in centrifuged oocytes. To allow unimpeded flux of dyes into the cytosol, oocytes were permeabilized with 0.01% Triton X-100 and then incubated 3 min with YO-PRO or ethidium (7.5 µM). The vehicle of YO-PRO and ethidium is also shown. Asterisks indicate the translucent zone in the animal pole. **(E)** Scheme of the TEVC/dye uptake assay. Oocytes were centrifuged to create a translucent zone in the animal pole. Then, oocytes were microinjected with 0.5 mg/ml salmon DNA to enhance the detection of polynucleotide-dependent fluorescent dyes. DAPI (100 µM) was coinjected to visualize the exogenous DNA. Finally, oocytes were placed in a chamber with the translucent zone (located in the animal pole) facing the objective of an inverted epifluorescence microscope. In parallel, the oocyte was impaled using the TEVC configuration to measure and control the membrane potential, as well as to determine the expression of exogenous large-pore channels by measuring the magnitude of ionic currents. Small fluorescent dyes were incubated or perfused using a gravity-dependent system. Dye uptake was recorded along the time course using a photomultiplier tube (PMT). **(F)** Concentration-response curve of ethidium uptake in translucent oocytes permeabilized with Triton X-100. Dye uptake experiments shown in D and F were performed using oocytes that did not express exogenous channels, at resting membrane potential (i.e., oocytes were not voltage-clamped), and perfused with a divalent cation-free Ringer solution.

To prevent contamination with nonspecific Ca^{2+}-activated endogenous currents, oocytes used for TEVC recordings were injected with 1,2-Bis(2-aminophenoxy)ethane-N,N,N′,N′-tetraacetic acid (BAPTA; final concentration, ~100 µM) 30 min before the recordings. To maintain plasma membrane integrity, BAPTA was not microinjected into oocytes selected for dye uptake measurements. Then, to eliminate contamination by currents mediated by endogenous Ca^{2+}-activated Cl^- channels, we applied repeated pulses

to negative potentials at the beginning of the experiments. This protocol has been shown to inactivate these currents (Eggermont, 2004; Hartzell et al., 2005; Kwon et al., 2013).

Quantification of kinetic parameters of molecular permeation

The expression of exogenous channels in *Xenopus* oocytes is variable. Therefore, to obtain accurate kinetic parameters of permeability, we normalized dye uptake rates to the activity of

functional channels at the cell surface. Thus, before dye uptake recordings, we quantified functional channel expression by the analysis of the peak tail current activated by a voltage-step pulse from –80 mV to 0 mV for 40 s. For connexins, ionic currents were analyzed at nominally zero Ca^{2+} (i.e., in divalent cation-free Ringer solution). In the case of CALHM1, ionic currents were recorded at 1 mM Ca^{2+}. In parallel, currents from non-injected oocytes (oocytes that did not express exogenous channels) were also recorded to determine the magnitude of any residual endogenous currents in oocytes from the same batch. Only batches of oocytes with negligible endogenous currents were used.

To normalize dye uptake to the current, we constructed correlation graphs of dye uptake rate (A.U./min) versus ionic current (μA). Each single point included in these graphs represents the dye uptake rate of an individual oocyte and the magnitude of the tail current recorded in the same oocyte before dye uptake measurement. These correlation graphs were made for each tested concentration of YO-PRO or ethidium (0.1, 1, 4, 7.5, 10, 15, and 25 μM). The resulting slopes from these graphs were calculated, plotted on a new concentration–response graph, and expressed as A.U./min × μA. To calculate the maximum transport (V_{max}) and the concentration of the transported molecule (dye) at which half-maximal transport is reached (K_m), normalized YO-PRO and ethidium uptake rates were fit to a Michaelis-Menten equation using Origin 9 software (OriginLab Corp.). Finally, oocytes with tail currents <1 μA were not considered in the analysis.

Molecular dynamics
Using our previous equilibrated human Cx26 model as a template (Luo et al., 2016), the homology model of human Cx30 hemichannel monomer was first constructed using the MED-ELLER program (Kelm et al., 2010), and then the hemichannel hexamer was built using the visual molecular dynamics program. The locations of V37, D50, I145, and D172/179 residues obtained in the Cx30 model are consistent with structural/functional data reported recently (Nielsen et al., 2017). The Cx30 hemichannel embedded in a solvated 1-palmitoyl-2-oleoyl phosphatidylcholine bilayer with 150 mM KCl and TIP3P (transferable intermolecular potential with three points) water molecules was built and equilibrated following the step-by-step protocol used in Membrane Builder on the CHARMM-GUI website (Jo et al., 2007). As in the Cx26 atomistic model, the terminal amino acid of each Cx30 segment was capped using the acetylated N-terminus and the methylated C-terminus (CT1), and three well-established disulfide bonds were added between the pairs of residues C53 and C180, C64 and C169, and C60 and C174 in each protomer. The whole simulation system contains 195,043 atoms, including 164 and 150 lipids in the upper and lower leaflets, respectively, and 114 K^+ and 144 Cl^- ions in solution. All atom simulations were performed using the AMBER 18 engine, and the CHARMM36m force field was used for proteins and lipids (Klauda et al., 2010; Best et al., 2012). For the 100-ns production run, temperature was maintained at 310.15 K using a Langevin thermostat; 1 atm was maintained by Monte Carlo barostat pressure control; and the time step was 2 fs. Long-range electrostatic interactions were calculated using the particle mesh Ewald algorithm (Darden et al., 1993). The cutoff for calculating van der Waals interactions and electrostatic interactions was set at 12 Å and force switched at 10 Å. The average and SD of the pore radius of Cx26 and Cx30 were calculated from the 40 snapshots evenly extracted from the last 40 ns using the Hole program (Smart et al., 1993).

Biotinylation and Western blotting
Eight oocytes expressing wild-type Cx30 or Cx30[G11R] were carefully placed in an Eppendorf tube and washed out with ND96 solution. Then, oocytes were incubated with HEN solution (composition in mM: 250 HEPES, 1 EDTA, and 0.1 neocuproine, adjusted to pH 7.7) containing 0.5 mg/ml EZ-Link Sulfo-NHS-SS-Biotin (catalog no. 21331; Thermo Fisher Scientific) for 20 min at 4°C. Subsequently, oocytes were washed out with PBS plus 15 mM glycine (pH 7.4) for 15 min. Oocytes were sonicated in HEN solution in the presence of protease inhibitors (catalog no. 1860932; Thermo Fisher Scientific) and then centrifuged for 10 min at 13,500 g and 4°C. Next, 10 μl from the supernatant were conserved for analysis of total Cx30, and the remaining supernatant was incubated with streptavidin agarose (catalog no. 20349; Thermo Fisher Scientific) for 60 min at 4°C. Samples were then centrifuged for 2 min at 14,000 g. The supernatant was discarded, and the fraction containing biotinylated proteins was washed out with HEN solution plus protease inhibitors. Then, samples were gently mixed with Laemmli buffer (Sigma-Aldrich) and heated for 5 min at 100°C to disrupt biotin–streptavidin interaction. Subsequently, total proteins and biotinylated proteins were separated by 12% SDS-PAGE and transferred onto a polyvinylidene difluoride membrane (Bio-Rad Laboratories). Signal Enhancer HIKARI (Nacalai Tesque, Inc.) was used to incubate the primary (catalog no. 71-2200, 1:1,000; Thermo Fisher Scientific) and secondary antibodies (catalog no. 32460, 1:5,000; Thermo Fisher Scientific). Super-Signal West Femto (Thermo Fisher Scientific) was used to detect the protein bands. Molecular mass was estimated with pre-stained markers (Bio-Rad Laboratories).

Reagents
MS-222, collagenase, penicillin-streptomycin, Ficoll, salmon DNA, HEPES, lanthanum chloride, ruthenium red, glycine, neocuproine, and ethidium bromide were purchased from Sigma-Aldrich. DAPI was obtained from Thermo Fisher Scientific. YO-PRO-1 iodide was acquired from Invitrogen.

Statistical analysis
Values are presented as mean ± SEM. Comparisons between groups were made using a paired or unpaired Student's t test or one-way ANOVA plus Newman-Keuls post hoc test as appropriate. $P < 0.05$ was considered significant.

Online supplemental material
Fig. S1 illustrates the effect of the antisense for Cx38 on ionic currents and dye uptake in *Xenopus* oocytes. Fig. S2 shows the effect of DAPI on ethidium intercalation to DNA. Fig. S3 shows the quantification of protein expression for Cx30 and Cx30[G11R].

Results

Centrifugation and DNA microinjection improve the visualization of polynucleotide-dependent fluorescent dyes

To facilitate optical detection of polynucleotide-dependent fluorescent molecules in *Xenopus* oocytes, we optimized a centrifugation protocol that renders the animal pole of oocytes translucent. Centrifugation created a *g* force–dependent translucent window in the animal pole by pulling yolk and pigment granules down toward the vegetal pole (Fig. 1 A). To confirm that the protocol improves optical visualization of fluorescent dyes, we microinjected DAPI (which fluoresces when bound to DNA) into the oocytes. As expected, in noncentrifuged oocytes, the fluorescence emitted by DAPI in the intracellular compartment was weak and diffuse (Fig. 1 B). In contrast, the DAPI-dependent fluorescent signal was clearer and more intense when it was visualized through the translucent zone of the centrifuged oocytes (Fig. 1, B and C). Coinjection of DAPI with salmon DNA significantly increased the intensity of the fluorescent signal, indicating that by increasing the DNA binding sites for DAPI, the dynamic range for detection of polynucleotide-dependent fluorescent dyes is enhanced (Fig. 1, B and C).

Next, we analyzed the ability to accurately detect influx of YO-PRO and ethidium, which, like DAPI, are small DNA-intercalator fluorescent molecules. To this end, we used permeabilized oocytes (see Materials and methods) preinjected with salmon DNA plus DAPI. Incubation of these oocytes in a solution containing YO-PRO or ethidium increased the fluorescent signal observed in the translucent animal pole (Fig. 1 D). As expected from previous observations in *Xenopus* oocytes, we detected autofluorescence at different wavelengths, but it was significantly lower than the fluorescent signal emitted by DAPI, YO-PRO, or ethidium (Fig. 1, B–D).

To increase the sensitivity of detection, we analyzed dye uptake with a photomultiplier tube instead of a conventional camera (Fig. 1 E). Using this setup, we found that the uptake of ethidium in the Triton X-100–permeabilized oocytes was linear as a function of concentration, indicating that the amount of DNA injected was sufficient to accurately report ethidium concentrations up to 50 µM without saturation (Fig. 1 F).

To analyze whether the centrifugation procedure and DNA/DAPI microinjection alter membrane permeability and electrochemical gradients, we measured resting membrane potentials in nontreated and in centrifuged/microinjected oocytes. We found that the procedure of centrifugation and subsequent DNA injection in *Xenopus* oocytes did not change the resting membrane potential (measured 2 h after DNA injection), including those oocytes overexpressing large-pore channels formed by CALHM1, Cx26, or Cx30 (Fig. 2 A).

To determine whether the procedure to make the oocytes translucent affects the gating of heterologously expressed channels, we analyzed the time course of currents activated by voltage in oocytes expressing CALHM1 or Cx26 in a solution containing 1.8 mM Ca²⁺. In control (noncentrifuged) oocytes, a single voltage pulse from –80 mV to 0 mV led to slowly activating currents, followed by tail currents with slow deactivation kinetics characteristic of these channels (Fig. 2 B). The ionic currents recorded in oocytes centrifuged and microinjected with DNA had similar activation and deactivation kinetics (Fig. 2 B), indicating that centrifugation and microinjection of exogenous DNA do not alter the voltage sensitivity of CALHM1 and Cx26. To test if the procedure of centrifugation and DNA injection affects Ca²⁺ sensitivity of CALHM1 and connexin hemichannels, we analyzed the activation of these channels at different concentrations of extracellular Ca²⁺. Notably, the magnitude of ionic currents recorded in control oocytes was similar to that recorded in centrifuged (translucent) oocytes (Fig. 2 C). Thus, our data indicate that the centrifugation and subsequent DNA microinjection do not modify the Ca²⁺ sensitivity of CALHM1 channels or connexin hemichannels.

The permeation of YO-PRO through the CALHM1 channel is saturable and Ca²⁺ and voltage dependent

Before performing TEVC/dye uptake experiments, CALHM1 expression in oocytes was confirmed by scanning for voltage-activated currents typically mediated by CALHM1 channels, which are kinetically distinguishable from noninjected oocytes. These ionic currents were fully blocked with 20 µM ruthenium red, a CALHM1 channel blocker (Fig. 3 A). We then studied YO-PRO permeability through CALHM1 channels at resting membrane potential in a divalent cation-free solution using the TEVC/dye uptake technique. The linear uptake of YO-PRO was clearly evident in oocytes that expressed CALHM1, and the rate of dye flux depended on the concentration of YO-PRO (Fig. 3 B). As expected, YO-PRO uptake was negligible in translucent oocytes that did not express CALHM1 (Fig. 3 C, black squares). Analysis of YO-PRO uptake rates measured in CALHM1-expressing oocytes revealed that the permeation of this molecule was saturable (Fig. 3 C).

In the presence of 1 mM extracellular Ca²⁺, resting membrane potentials in noninjected and CALHM1-expressing oocytes were –37.6 ± 1.2 mV and –15.6 ± 0.6 mV, respectively (P < 0.0001). The resting membrane potential of oocytes expressing CALHM1 was close to the reversal potential described previously by others under similar experimental conditions (Siebert et al., 2013), suggesting that these channels have a nonzero, small open probability at resting membrane potential in the presence of 1 mM extracellular Ca²⁺. The presence of 1 mM Ca²⁺ in the extracellular solution decreased but did not abolish the YO-PRO uptake (Fig. 3 C). In addition, 20 µM ruthenium red fully prevented the uptake of 25 µM YO-PRO in CALHM1-expressing oocytes exposed to a bath solution containing either 1 mM Ca²⁺ or zero Ca²⁺ (Fig. 3 D).

Theoretically, dye uptake depends on channel expression and channel activity (e.g., open probability). Consistent with this notion, YO-PRO uptake strongly correlated with the magnitude of peak tail currents mediated by CALHM1 channels (Fig. 3 E). To control variability in channel expression, dye uptake was normalized to the tail current of CALHM1 recorded in the same oocyte. By fitting the data to a Michaelis-Menten equation, we obtained an accurate and reliable quantification of kinetic parameters for YO-PRO transport, showing that 1 mM extracellular Ca²⁺ decreased V_{max} by almost half (0.180 ± 0.0063 versus 0.094 ± 0.0056 A.U./min × µA) without significantly changing the apparent K_m (7.50 ± 1.24 versus 8.58 ± 0.24 µM; Fig. 3 F).
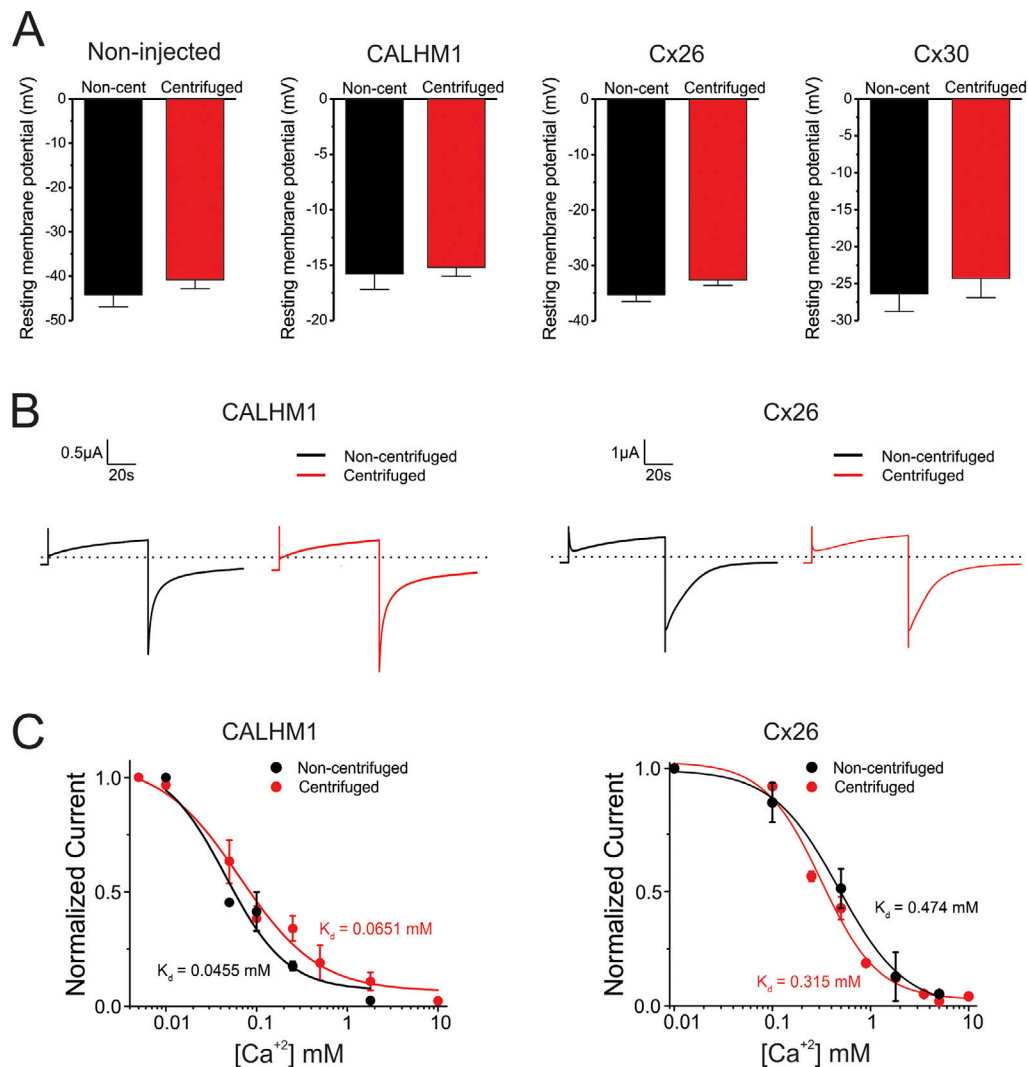
Figure 2. **Centrifugation and DNA injection do not affect the biophysical properties of CALHM1 channels and connexin hemichannels. (A)** Resting membrane potentials recorded in noncentrifuged (Non-cent) and centrifuged oocytes. Values were obtained from oocytes perfused with Ringer solution in the presence of 1.8 mM extracellular Ca^{2+}. Membrane potentials were measured in noninjected oocytes and in oocytes expressing CALHM1, Cx26, or Cx30. **(B)** Representative current traces recorded during a voltage pulse (step) from −80 mV (holding potential) to 0 mV in CALHM1- or Cx26-expressing oocytes. The dashed line indicates 0 μA. Currents were measured in a Ringer solution containing 1.8 mM Ca^{2+}. **(C)** Effect of extracellular Ca^{2+} on voltage-activated currents mediated by CALHM1 channels or Cx26 hemichannels. Tail currents were recorded using voltage-step pulses from −80 mV (holding potential) to 0 mV; duration step, 40 s. For experiments shown in B and C, oocytes were microinjected with BAPTA. Data in C were fit to a Hill equation to obtain K_d values. Error bars are SEM.

Next, we explored the voltage dependence of atomic ion flux and molecular permeation in CALHM1 channels. In the absence of divalent cations, a high conductance was detected at both negative and positive membrane potentials (Fig. 4, A and B, red circles). Notably, at 1 mM extracellular Ca^{2+}, ionic currents were negligible at potentials more negative than +20 mV (Fig. 4, A and B, black circles). At 1 mM extracellular Ca^{2+}, YO-PRO uptake progressively increased as membrane potential was clamped at more positive values, despite the fact that electrochemical gradient for YO-PRO is lower at positive membrane potentials (Fig. 4 B, black triangles). Voltage dependence of YO-PRO uptake and ionic currents did not overlap. Indeed, YO-PRO uptake was detected at voltages more negative than +20 mV, suggesting that molecular transport occurred even when there was no or low

detectable atomic ion permeation (Fig. 4 B). Further analysis of ionic currents and the V_{max} of YO-PRO at resting membrane potential revealed that 1 mM extracellular Ca^{2+} inhibited ∼95% of ionic currents but only ∼48% of YO-PRO uptake (Fig. 4 C). Removal of Ca^{2+} from the extracellular bath increased ∼20-fold the ionic currents but only ∼2-fold the maximum transport of YO-PRO (Fig. 4 D). Thus, changes in the V_{max} do not correlate with changes in the relative open probability of the channels.

Cx30 hemichannels also display saturable molecular transport
To evaluate if other large-pore channels display saturating transport to molecules, we analyzed molecular permeability in translucent oocytes expressing connexin hemichannels. To assess molecular permeation through connexin hemichannels, we
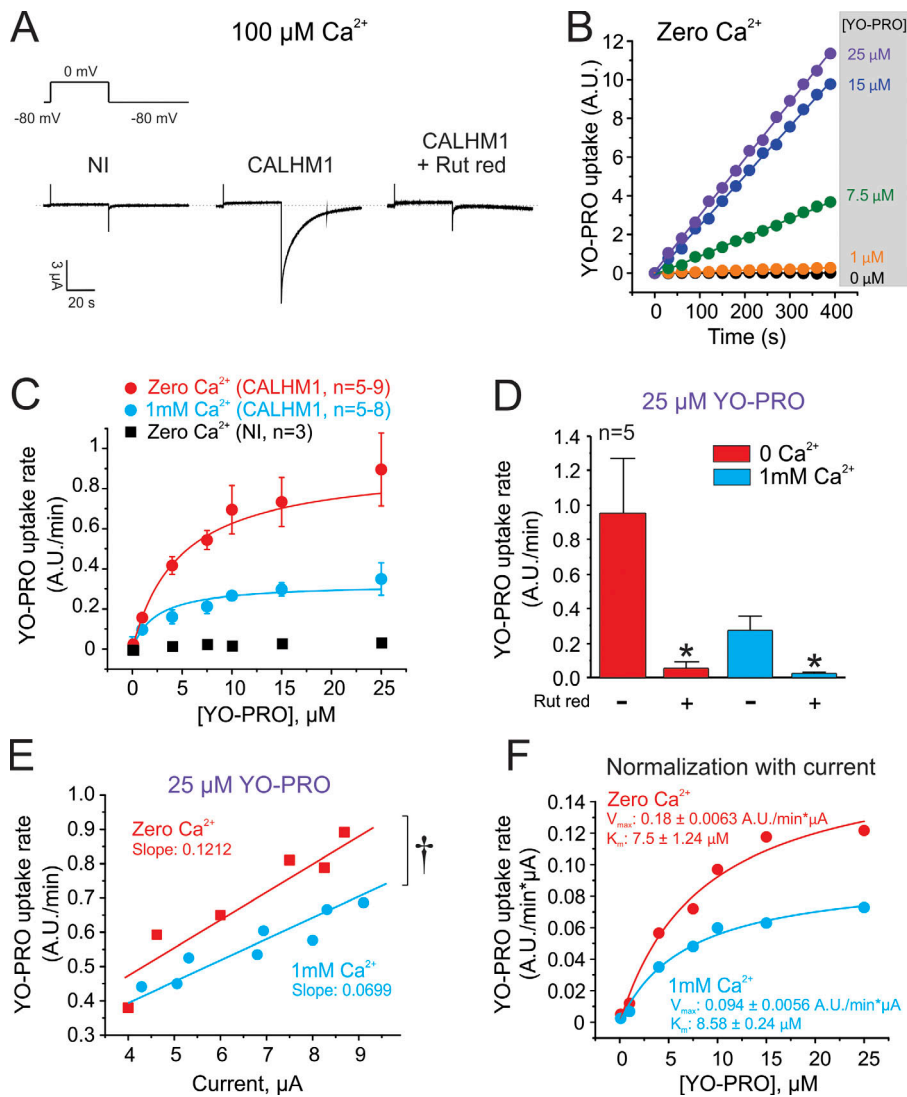
Figure 3. The TEVC/dye uptake assay reveals that YO-PRO permeation through CALHM1 channels is saturable and Ca^{2+} sensitive. (A) Representative current traces recorded in oocytes expressing CALHM1 incubated with Ringer solution containing 100 µM Ca^{2+}. The effect of 20 µM ruthenium red (Rut red), a CALHM1 blocker, is shown. The dashed line indicates 0 µA. NI, noninjected. **(B)** Representative time course of YO-PRO uptake in oocytes expressing CALHM1. Recordings were performed in a divalent cation-free Ringer solution and at resting membrane potential. **(C)** Analysis of YO-PRO uptake rates in NI oocytes (black squares) or in oocytes expressing CALHM1 (circles). YO-PRO uptake was evaluated in a divalent cation-free Ringer solution or in the presence of 1 mM extracellular Ca^{2+}. All measurements were performed at resting membrane potential. **(D)** The uptake of 25 µM YO-PRO at resting membrane potential is inhibited by 20 µM Rut red. *, P < 0.05 versus control by one-way ANOVA plus Newman-Keuls post hoc test. **(E)** YO-PRO uptake rate is correlated to CALHM1 expression (determined as the magnitude of the tail current measured before dye uptake recording). †, P < 0.05 by t test. **(F)** YO-PRO uptake rates shown in C were normalized by CALHM1 expression (see Materials and methods). Data in F were fit to a Michaelis-Menten equation to obtain V_{max} and K_m. Error bars are SEM.

used ethidium as a molecular tracer because it has been used extensively as a fluorescent dye to analyze connexin hemichannel/GJC activity. Consistent with previous findings (Hansen et al., 2014a, 2014b; Nielsen et al., 2017), we detected ethidium uptake at resting membrane potentials through Cx30 hemichannels but not through Cx26 hemichannels (Fig. 5 B). Thus, we further characterized the permeability of ethidium through Cx30 hemichannels. Resting membrane potentials in noninjected oocytes and in those expressing Cx30 were –38.4 ± 0.9 mV and –30.5 ± 0.9 mV, respectively (P < 0.001). The ionic currents recorded in Cx30-expressing oocytes were abolished by 200 µM La^{3+}, a connexin blocker (Fig. 5 A). Also, ethidium uptake in Cx30-expressing oocytes was fully prevented by 200 µM La^{3+} (Fig. 5 B). As expected, the magnitude of the uptake rate through Cx30 hemichannels was dependent on ethidium concentration (Fig. 5, B and C). Importantly, ethidium uptake in translucent oocytes that did not express Cx30 was negligible in the absence of divalent cations (Fig. 5, B and C). Analysis of the ethidium uptake rates revealed that transport of this molecule through Cx30 hemichannels was saturable at micromolar concentrations (Fig. 5 C). Similar to the observations in CALHM1-

expressing oocytes, ethidium uptake correlated with the magnitude of Cx30 tail currents (Fig. 5 D). The normalization of dye uptake to the tail current evoked by Cx30 channel opening confirmed that ethidium permeation was saturable with a V_{max} = 0.078 ± 0.015 A.U./min × µA and apparent K_m = 8.10 ± 1.65 µM (Fig. 5 E). Overall, our data confirm that Cx30 displays properties of saturating transport similar to that observed for CALHM1 channels.

Mutations in the N-terminal region of connexin hemichannels affect the selectivity and transport

Cx26 is the most closely related isoform to Cx30, sharing >90% sequence similarity in the pore region. However, in contrast to Cx30, ethidium was not permeable through Cx26 hemichannels, suggesting that permselectivity properties are quite different in these similar connexin isoforms. We built a homology model of Cx30 based on our equilibrated and previously validated Cx26 model (Fig. 6, A and B; Luo et al., 2016). The Cx30 model is consistent with structural/functional data reported previously (Nielsen et al., 2017). The pore radius after 100-ns simulation shows that Cx30 is actually narrower than Cx26 at several points
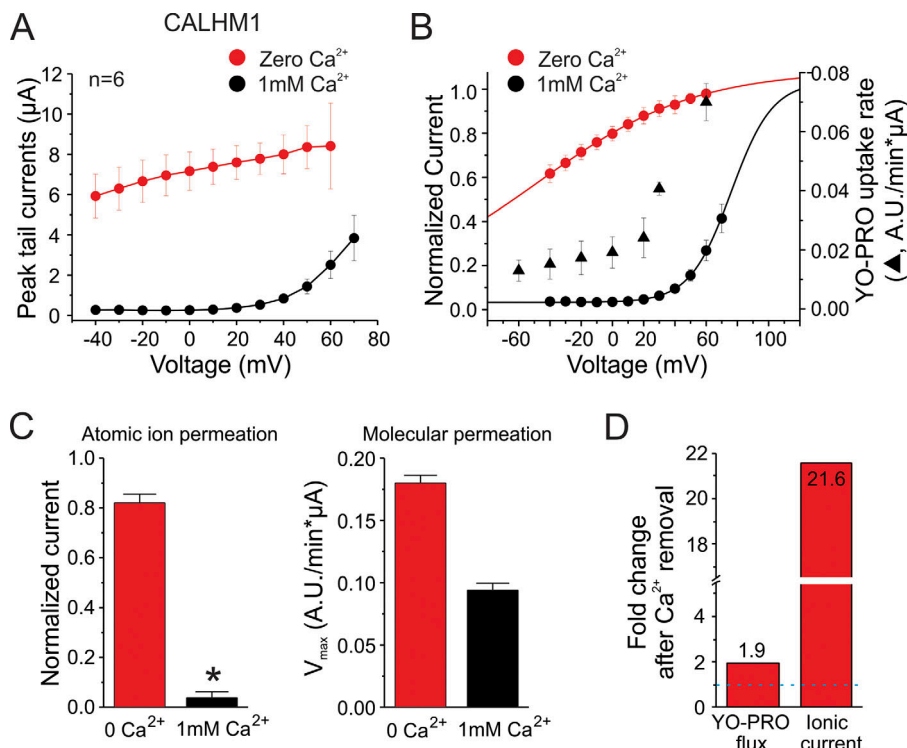
Figure 4. Voltage dependence of YO-PRO uptake reveals that permeability of molecules and ionic currents in CALHM1 channels are differentially affected. (A) I-V relationship of CALHM1 channels. Oocytes were clamped at a holding potential of −80 mV, and depolarizing-step pulses from −40 mV to +70 mV were applied. The ionic current was evaluated in a divalent cation-free Ringer solution (red circles) or in the presence of 1 mM extracellular Ca^{2+} (black circles). For these experiments, oocytes were microinjected with BAPTA. **(B)** Voltage dependence of YO-PRO uptake (triangles). The uptake of 7.5 µM YO-PRO was evaluated at different controlled membrane potentials in the presence of 1 mM extracellular Ca^{2+}. Dye uptake was recorded in clamped oocytes during 10 min to calculate dye uptake rates. The current shown in A was normalized to the current recorded in divalent cation-free Ringer solution. **(C)** Analysis of the effect of 1 mM extracellular Ca^{2+} on the ionic currents (atomic ion permeation) and the maximum flux of YO-PRO (molecular permeation), both measured at resting membrane potential. *, P < 0.05 versus 0 Ca^{2+} by paired Student's *t* test. **(D)** Change in YO-PRO flux and ionic currents after Ca^{2+} removal from the extracellular bath illustrates the differential effect of Ca^{2+} on atomic ion permeation versus molecular permeation. Numbers indicate the fold change value. Error bars are SEM.

along the pore (Fig. 6 C). Thus, simple steric considerations cannot account for the impermeability of Cx26 to ethidium. The structure and sequence comparison shows that the pore-lining region in Cx26 and Cx30 mostly differs at the short N-terminal helix, which is also the most flexible element of the pore (Fig. 6 A). This suggests that the difference in ethidium permeability arises from different channel–ligand interactions and the dynamics of the pore with a permeant present.

Hence, we used the TEVC/dye uptake assay to determine the effect of pathogenic human connexin mutations in the N-terminal region on ethidium transport across the cell membrane. We first analyzed the human mutation G11R in Cx30, which produces hidrotic ectodermal dysplasia (Zhang et al., 2003; Essenfelder et al., 2004; Chen et al., 2010). Consistent with the gain of function proposed for this mutation, the voltage-activated currents in oocytes expressing Cx30[G11R] were higher than with wild-type Cx30 (Fig. 6 D). The increase of ionic currents was not associated with an increase of Cx30[G11R] channels in the plasma membrane (Fig. S3), suggesting that the mutation G11R increases the open probability of the channel and/or the conductance to atomic ions. As seen previously, ethidium uptake in wild-type Cx30-expressing oocytes was detectable at resting membrane potential and correlated with the magnitude of voltage-activated tail currents of Cx30 hemichannels (Fig. 6 E). Strikingly, ethidium uptake in Cx30[G11R] was not detected even when high Cx30[G11R]-mediated currents were detected (Fig. 6 E).

We then evaluated the human mutation N14K in Cx26, which is also associated with gain in function and produces deafness

and skin disorders (van Steensel et al., 2004; Lazic et al., 2008; Lee et al., 2009; Valdez Capuccino et al., 2019). The N14K mutation does not affect channel expression levels but leads to an increase of the open probability of Cx26 hemichannels by disrupting interactions between subunits (Lee et al., 2009; Valdez Capuccino et al., 2019). Consistent with this, the ionic current recorded in oocytes expressing Cx26[N14K] was higher than for wild-type Cx26 (Fig. 6 F). As reported above, ethidium uptake in wild-type Cx26-expressing oocytes was negligible in a divalent cation-free Ringer solution at resting membrane potential and did not correlate with the magnitude of tail currents mediated by Cx26 hemichannels (Figs. 5 B and 6 G). In contrast, ethidium uptake was observed in Cx26[N14K]-expressing oocytes, and it was directly proportional to the magnitude of tail currents mediated by Cx26[N14K] hemichannels (Fig. 6 G). Together, these data strongly support the notion that atomic ion permeation and molecular permeability are not necessarily coupled in connexin channels, and mutations at the N-terminal region could significantly affect transport of molecules and/or selectivity (i.e., permselectivity).

Discussion

Large-pore channels such as those formed by connexin, pannexin, and CALHM1 are permeable to both atomic ions and small molecules. Although atomic ion permeation properties through these channels are accurately assessed using electrophysiological approaches, the study of molecular selectivity and molecular permeation has been limited by qualitative techniques that only
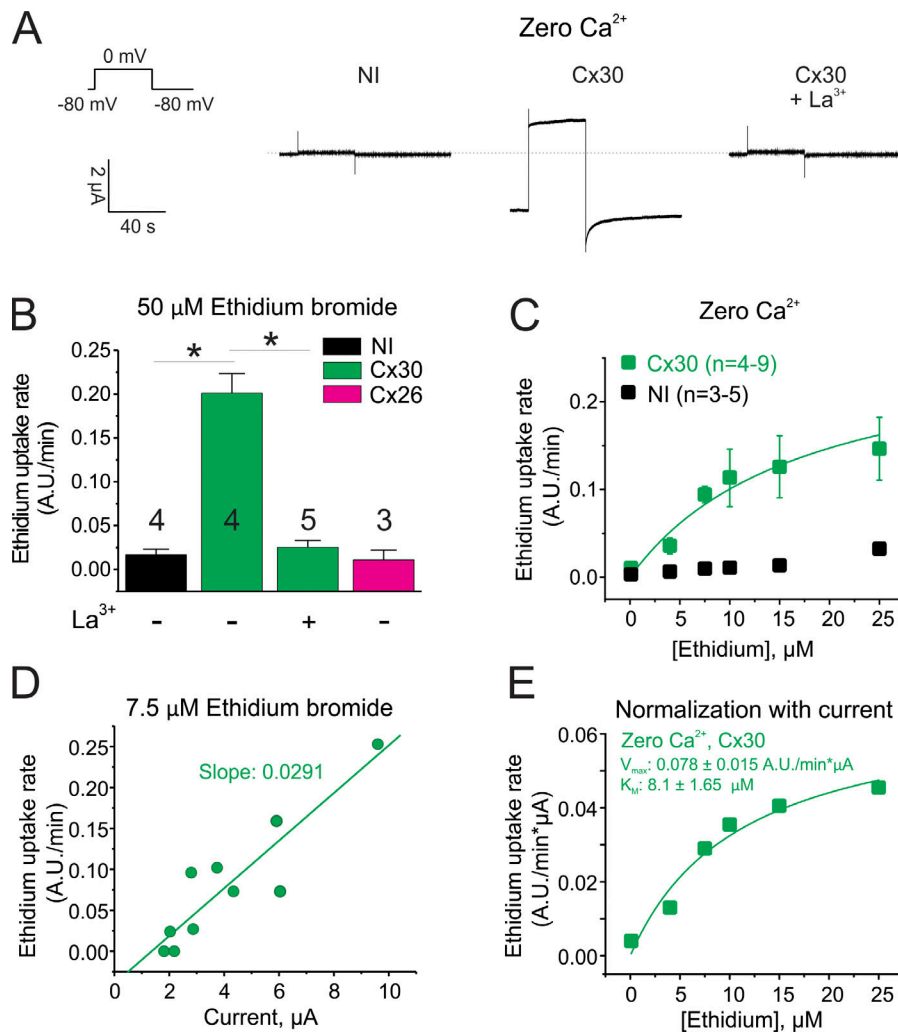
Gaete et al.
Saturating transport in large-pore channels

Journal of General Physiology
https://doi.org/10.1085/jgp.202012607

9 of 15

Figure 5. **Ethidium permeation through Cx30 hemichannels is saturable and has quantifiable kinetic properties. (A)** Representative current traces recorded in oocytes expressing Cx30 incubated with a divalent cation-free Ringer solution. The effect of 200 µM La^{3+}, a connexin hemichannel blocker, is shown. The dotted line indicates 0 µA. NI, noninjected. **(B)** Ethidium uptake rates detected in NI oocytes or in oocytes expressing Cx30 and Cx26. In these experiments, dye uptake was measured in oocytes incubated with a divalent cation-free Ringer solution plus 50 µM ethidium bromide. Ethidium uptake was evaluated at resting membrane potential in the absence or presence of 200 µM La^{3+}. *, P < 0.05 by one-way ANOVA plus Newman-Keuls post hoc test. **(C)** Ethidium uptake rates measured in oocytes stimulated with a divalent cation-free Ringer solution at resting membrane potential. Ethidium uptake was evaluated in oocytes expressing Cx30 (green squares) and in NI oocytes, which do not express Cx30 (black squares). **(D)** Ethidium uptake is correlated to Cx30 expression (determined as the magnitude of the tail current measured before dye uptake recording). **(E)** Kinetic parameters of ethidium uptake after normalization of data shown in C by Cx30 expression (see Materials and methods). Data were fit to a Michaelis-Menten equation to obtain V$_{max}$ and K$_m$. Error bars are SEM.

allow assessing molecular transport at resting or noncontrolled membrane potentials. Here, we report a novel technique that allows the study of permselectivity to fluorescent dyes under controlled membrane potentials in *Xenopus* oocytes. With this methodology, we succeeded in analyzing the voltage dependence of molecular transport and obtained accurate kinetic parameters of permeability in CALHM1 channels and Cx30 hemichannels. In addition, we distinguished new biophysical properties that support the hypothesis that molecular permeation is selective, saturable, and not necessarily directly correlated with changes in atomic ion permeability through the conduction pathway of large-pore channels, and can even be oppositely correlated.

Development of a novel technique to analyze molecular transport through large-pore channels

Detection of fluorescence in oocytes is particularly challenging because of the pigments located in the cytosol of the animal pole and the high content of yolk granules that restrict the transmission of fluorescent signals from the intracellular compartment (Dumont, 1972). Therefore, we optimized and characterized a centrifugation-based protocol initially described by Iwao et al. (1997) to quantify the cytoplasmic volume of nonfertilized oocytes. Oocyte centrifugation at 4,000 g was

shown to form a translucent cytoplasmic window by pulling down the yolk and pigment granules but affected cell morphology (Iwao et al., 1997). In our experience, g forces ≤3,000 g created a translucent window in the animal pole without affecting the cell morphology. After the centrifugation step, the subsequent microinjection of DNA and DAPI led, in some cases, to leakage of cytoplasmic content from the sites where microinjections were done. It is important to note that the leakage was observed only in oocytes centrifuged at g forces >1,700 g. The last observation suggests that higher centrifugation forces could weaken the plasma membrane. Therefore, to avoid affecting cell morphology and to retain plasma membrane integrity, we decided to render translucent oocytes using ≤1,700 g for all the TEVC/dye uptake experiments.

Centrifugation at 1,700 g and subsequent microinjection of DNA did not affect the plasma membrane integrity because resting membrane potential remained unchanged and stable at the time when experiments were performed, and oocytes were impermeable to the small charged dyes YO-PRO and ethidium when they did not express exogenous large-pore channels. The presumption that cell function is conserved after the procedure is supported by a previous report showing that the centrifugation of fertilized oocytes at 650 g did not affect their viability or
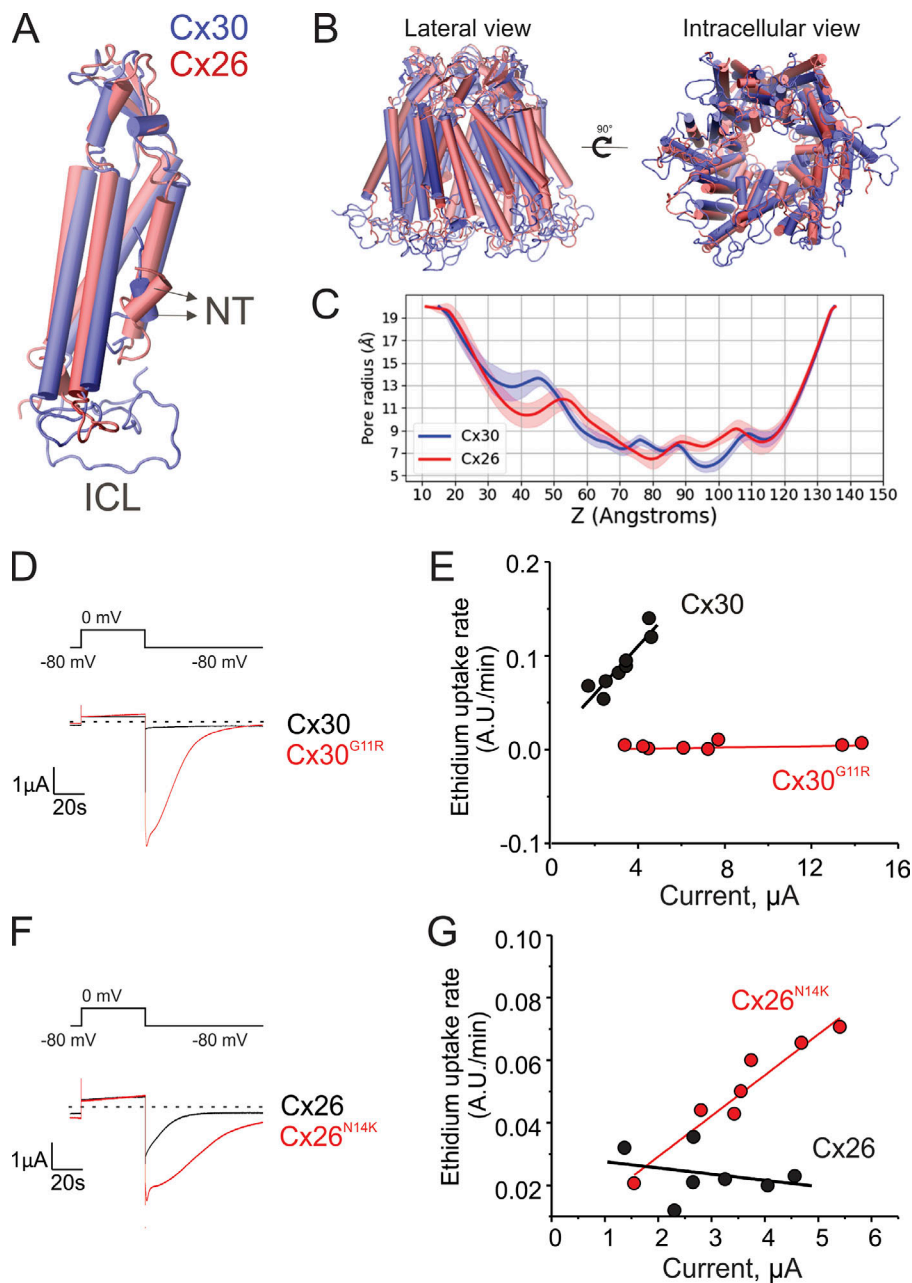
Figure 6. **The N-terminal region is a major determinant of the permselectivity of ethidium in connexin hemichannels. (A)** Comparison of Cx30 and Cx26 monomers shows differences in the N-terminal domain (NT) and the intracellular loops (ICLs). **(B)** Molecular reconstruction of Cx30 hemichannels reveals high similarity to hemichannels formed by Cx26. Cx30 and Cx26 hemichannels are colored with blue and red, respectively. **(C)** Assessment of pore diameter of MD-equilibrated Cx26 and Cx30 hemichannels indicates similar pore width. **(D)** Voltage-activated current in oocytes expressing wild-type Cx30 (black trace) or Cx30^{G11R} (red trace). The horizontal dashed line indicates 0 µA. **(E)** Ethidium uptake rates measured in oocytes expressing different levels of wild-type Cx30 (black circles) or Cx30^{G11R} (red circles). **(F)** Voltage-activated current in oocytes expressing wild-type Cx26 (black trace) or Cx26^{N14K} (red trace). The horizontal dashed line indicates 0 µA. **(G)** Ethidium uptake rates obtained from oocytes with different expression levels of wild-type Cx26 (black circles) or Cx26^{N14K} (red circles). Wild-type Cx30 is permeable to ethidium, but the mutation G11R eliminates permeability to this dye. In contrast, wild-type Cx26 is not permeable to ethidium, but the mutation N14K turns the channel permeable to this molecule. The ionic currents shown in D and F were recorded from oocytes perfused with a Ringer solution containing 1 mM Ca^{2+}, using a voltage-step pulse from −80 mV to 0 mV. For experiments shown in D and F, oocytes were injected with the same amount of cRNA. Dye uptake experiments were performed at resting membrane potential, using 7.5 µM ethidium bromide in the bath solution, and at zero extracellular Ca^{2+}. Tail currents shown in E and G were obtained using a voltage-step pulse from −80 mV to 0 mV (40 s at zero extracellular Ca^{2+}) before ethidium uptake measurements (see Materials and methods).

division capability (Iwao et al., 2005). Notably, we observed that viability is not altered for ≥2–3 d after centrifugation and DNA microinjection, and, most importantly, we demonstrated that this procedure did not affect the biophysical properties of expressed exogenous channels.

Oocytes have a variable intrinsic autofluorescence, which may limit the use of fluorescence to study heterologously expressed ion channels (Lee and Bezanilla, 2019). However, in our translucent oocytes, the fluorescence emitted by the interaction of DAPI, YO-PRO, or ethidium with exogenous salmon DNA in the intracellular compartment was easily distinguished from autofluorescence.

In the TEVC/dye uptake assay, molecular permeability is assessed by using fluorescent dyes that intercalate with DNA. Therefore, saturation of the signal could occur by a reduction of free binding sites in the DNA contained by the oocytes. We avoided this possibility by injecting exogenous DNA into the oocyte to enhance the number of binding sites. The coinjection of DNA with DAPI did not significantly affect the binding capacity for ethidium (Fig. S2), and, most importantly, we observed a linear relationship between fluorescent dye uptake and its concentration in permeabilized cells over the range of concentrations used (Fig. 1 F). Thus, we confirmed that binding sites do not saturate in our assay.

Analysis of quantitative parameters for molecular transport through large-pore channels

Saturation of molecular flux was proposed for hemichannels formed by Cx43 in HeLa cells (Orellana et al., 2011). Using the TEVC/dye uptake assay, we found that CALHM1 channels and

Gaete et al.
Saturating transport in large-pore channels

Journal of General Physiology
https://doi.org/10.1085/jgp.202012607

11 of 15

Cx30 hemichannels showed saturable transport for YO-PRO and ethidium, respectively. Surprisingly, the saturation of transport was observed at the low micromolar range, suggesting that these channels behave in some ways like molecular transporters. Interestingly, the quantification of kinetic parameters for the molecular transport in CALHM1 revealed that extracellular Ca^{2+}, a well-known regulator of CALHM1 gating, did not affect apparent K_m but did affect V_{max}. These data indicate that Ca^{2+} did not affect the apparent affinity of the channel for YO-PRO, but rather maximal molecular flux, probably as a consequence of the decrease in the open probability or the mean open time.

Our data showing molecular permeation through CALHM1 channels in the presence of 1 mM extracellular Ca^{2+} differ from data in another study addressing CALHM1 permeability by fluorescent dye uptake. In contrast to our results, Siebert et al. (2013) did not detect dye uptake with 5 mM Ca^{2+} in the extracellular bath solution. The reason for this discrepancy could rely on the experimental conditions used and most likely on the extracellular Ca^{2+} concentration, which in our case is 1 mM. Consistent with this notion, ATP release from HeLa cells expressing CALHM1 has been detected when Ca^{2+} concentrations are ≤0.9 mM (Taruno et al., 2013). Furthermore, the half-maximal inhibitory concentration value for Ca^{2+}-dependent inhibition of ATP release was estimated at 495 µM, suggesting that molecular flux through CALHM1 channels is not restricted to Ca^{2+}-free conditions (Taruno et al., 2013).

Because flux is directly related to channel expression (Contreras et al., 2003; Retamal et al., 2007; Schalper et al., 2008, 2010; Orellana et al., 2011; García et al., 2015), normalization of dye uptake to the number of functional channels located at the plasma membrane is essential to determine accurate kinetic parameters of permeation. Consequently, fluorescently tagged channels have been used to estimate the relative channel expression in parallel to functional channel assays (Orellana et al., 2011). The use of fluorescent tags for this purpose, however, has significant limitations. First, it requires tagging the target protein with a fluorescent reporter protein, which could affect the gating or permselectivity properties (Bukauskas et al., 2001; Limon et al., 2007; Huang et al., 2011; Gaitán-Peñas et al., 2016). Second, analysis of the fluorescent signal emitted from the plasma membrane is complicated and could be subjective because analysis is performed from one simple focus (z axis), and hemichannels need not be uniformly distributed in the plasma membrane, as previously reported for CALHM1/3, Cx43, Cx26, and Cx32 (Nakagawa et al., 2011; Orellana et al., 2011; García et al., 2015; Kashio et al., 2019). Third, nonfunctional or silent channels will be incorporated in the quantification of fluorescently labeled proteins.

To obtain a quantitative measure of the permeability pathway offered by the channels under study, and to avoid the limitations associated with fluorescent reporters, we determined channel currents by TEVC in the same oocytes in which dye uptake experiments were performed. This current reflects the number of functional channels and their aggregate open probability under each experimental condition, allowing accurate normalization of molecular permeability. However, if the mechanisms of transport for ions and molecules are distinct,

meaning that some channels differentially transport ionic atoms and molecules, electrophysiological techniques measuring ionic currents could not detect those molecule-preferring channels. Yet, we expect that the proportion of channels with different permeabilities to atomic ions and molecules will remain the same, independent of the levels of channel expression. Thus, the detected amount of ionic permeable channels should reflect the relative number of molecule-permeable channels. This notion is supported by our experiments showing a strong correlation between the magnitude of the ionic currents and the rate of dye uptake in the oocytes that expressed all the dye-permeable channels that we tested (CALHM1, Cx30, and Cx26[N14K]). Importantly, the proportion between ionic and molecule-permeable channels might change within the same oocyte if conditions that control gating are modified. Therefore, tail currents used for normalization must be obtained in the same condition for all oocytes expressing a particular channel.

Molecular permeability can be assessed at defined membrane potentials

In addition to allowing reliable quantification of functional channel expression in parallel with the molecular permeability assay, the simultaneous use of TEVC and a dye uptake assay has two important advantages for the study of permeation of molecules through large-pore channels. First, the TEVC configuration permits the identification of healthy oocytes (i.e., those with an intact plasma membrane) by recording stable currents and resting membrane potentials before and throughout the experiment. Second, the control of the membrane potential allows determination of permselectivity and kinetic parameters in cells at specific/controlled membrane potentials. Thus, the TEVC/dye uptake assay enables analysis of the voltage dependency of molecular transport through large-pore channels. Until now, the study of molecular transport through large-pore channels has been performed mostly at resting membrane potentials, at which membrane potential are often not measured or well controlled due to technical limitations. This methodology will contribute to addressing relevant questions related to the regulation by voltage of the transport in large-pore channels, which might be particularly important for those channels expressed in excitable cells.

It should be noted that for voltage-controlled permeation assays, oocytes must be voltage clamped for minutes. Holding of membrane potential at very positive voltages is difficult, even in the presence of extracellular Ca^{2+}. Nevertheless, the holding potentials used to assess molecular permeation were stable, even when currents did not always reach steady state.

Due to frequent coexpression of large-pore channels in cells from intact tissue and overlapping pharmacology profiles, heterologous expression systems are the most appropriate models to study the biophysical properties (gating and permeability) of large-pore channels. Specifically, the use of the TEVC technique in oocytes has been shown to be particularly appropriate for the characterization of gating kinetics of large-pore channels (Bruzzone et al., 2005; Ma et al., 2012; Capuccino and Contreras, 2016; Gaitán-Peñas et al., 2016; Lopez et al., 2016; Tanis et al., 2017; Valdez Capuccino et al., 2019). The TEVC/dye uptake

technique can only be used in large cells; mammalian cells are not suitable for this methodology, and alternative techniques such as patch-clamp fluorometry should be adapted for those cells.

Implications for the relationship between molecular and atomic ion permeation

The conventional view of wide-pore channels is that both atomic ions and molecules diffuse freely through the pore following their electrochemical gradients. In this view, the activation/opening of large-pore channels should proportionally increase the flux of both atomic ions and small molecular permeants, as reported early for GJCs (Verselis et al., 1986; Kanaporis et al., 2011). However, from the data obtained using the TEVC/dye uptake assay, we suggest that this correlated permeation may not apply to large-pore channels.

We found that, in the presence of extracellular Ca^{2+}, ionic currents through CALHM1 channels are observed mostly at positive membrane potentials, whereas significant YO-PRO permeation was detected at negative potentials at which negligible current was detected. Furthermore, the voltage dependence of YO-PRO uptake did not overlap with the I-V relationship of CALHM1 channels, supporting that atomic ion flux is somehow uncoupled from molecular permeation. The lack of correlation between atomic ion permeability and molecular transport has been reported previously for other large-pore channels. For example, significant Cx43-mediated ethidium permeability was reported at negative resting membrane potential where no atomic ion currents were detected even at the single-channel level (Contreras et al., 2003; Hansen et al., 2014a, 2014b). Recently, the same phenomenon was observed in pannexin-1 channels (Nielsen et al., 2020).

The permeation of atomic ions and tetraalkylammonium cations through CALHM1 channels has been suggested to depend mainly on the permeant size (Siebert et al., 2013). However, our results indicate that other determinants may be involved, depending on the nature of the transported molecule.

The notion that molecular permeation does not directly correlate with, or cannot even be predicted from, atomic ion–dependent currents in large-pore channels is supported by our findings in Cx30-expressing oocytes as well. Cx30 hemichannels are well-known ethidium-permeable channels (Hansen et al., 2014a, 2014b; Nielsen et al., 2017), but a single mutation in the N-terminal region associated with a considerable gain of atomic ion permeation fully restricted the molecular permeation. Consistent with this, alterations in the putative pore residue V37 of Cx30 increase atomic ion flux without altering permeability to ethidium (Nielsen et al., 2017). Interestingly, some pharmacological blockers of connexin or pannexin channels can selectively inhibit atomic ion permeation but not molecular uptake (Nielsen et al., 2019, 2020). Consistently, we found that 1 mM extracellular Ca^{2+} reduces ~95% of ionic current but only half of the YO-PRO permeation through CALHM1 channels.

The structure of the N-terminal region of large-pore channels has been difficult to resolve, but recent evidence suggests that N-terminal residues are oriented into the pore (Maeda et al., 2009; Deneka et al., 2018; Kasuya et al., 2018; Myers et al., 2018; Choi et al., 2019; Demura et al., 2020; Michalski et al., 2020; Syrjanen et al., 2020). The structural data suggest that the N-terminus is a flexible structure with a potential role in the control of gating and/or permselectivity. In line with this hypothesis, modification of the N-terminus alters voltage sensitivity, permeability to molecules, or gating properties in pannexin, connexin, and CALHM channels (Tanis et al., 2017; García et al., 2018; Michalski et al., 2018; Choi et al., 2019; Valdez Capuccino et al., 2019; Demura et al., 2020). Notably, we observed that the N-terminus is essential for controlling permselectivity to ethidium in Cx26 and Cx30 hemichannels. Consistent with this, the replacement of the N-terminus of Cx43 (ethidium permeable) with the N-terminus of Cx30 does not affect the permeability to ethidium (Nielsen et al., 2019).

Using molecular dynamic simulations, we found that the diameter of the permeation pathway in Cx30 hemichannels is similar to the pore size of Cx26 hemichannels, even though the permselectivity properties of Cx26 and Cx30 are quite different. Thus, the width of the pore may not be the major determinant for the permeation of molecules, but rather the nature of the residues lining the pore and the interactions of the permeant with them. Saturation of molecular permeation indicates that interactions of permeants with binding sites in the permeation pathway could determine the permselectivity through large-pore channels. Altogether, this evidence supports the hypothesis that large-pore channels are not free diffusion pores for molecules, and distinct mechanisms for atomic ion and molecular transport coexist (Gaete and Contreras, 2020; Nielsen et al., 2020).

In summary, we report a novel and simple technique that combines electrophysiology and the fluorescence of DNA intercalator dyes to analyze in the same cell the molecular permeability and the atomic ion flux through large-pore channels. The potential use of our TEVC/dye uptake assay could reveal important insights regarding the specific mechanisms of molecular and atomic ion permeability of large-pore channels in health and disease.

Acknowledgments

References

Best, R.B., X. Zhu, J. Shim, P.E. Lopes, J. Mittal, M. Feig, and A.D. Mackerell Jr. 2012. Optimization of the additive CHARMM all-atom protein force field targeting improved sampling of the backbone φ, ψ and side-chain χ(1) and χ(2) dihedral angles. *J. Chem. Theory Comput.* 8:3257–3273. https://doi.org/10.1021/ct300400x

Bruzzone, R., M.T. Barbe, N.J. Jakob, and H. Monyer. 2005. Pharmacological properties of homomeric and heteromeric pannexin hemichannels expressed in *Xenopus* oocytes. *J. Neurochem.* 92:1033–1043. https://doi.org/10.1111/j.1471-4159.2004.02947.x

Bukauskas, F.F., A. Bukauskiene, M.V. Bennett, and V.K. Verselis. 2001. Gating properties of gap junction channels assembled from connexin43 and connexin43 fused with green fluorescent protein. *Biophys. J.* 81:137–152. https://doi.org/10.1016/S0006-3495(01)75687-1

Capuccino, J., and J. Contreras. 2016. Functional characterization of connexin hemichannels using *Xenopus* oocytes and the two-electrode voltage clamp technique. *In* Gap Junction Channels and Hemichannels. D. Bai and J.C. Sáez, editors. CRC Press, Boca Raton, FL. 203–214.

Chen, N., C. Xu, B. Han, Z.Y. Wang, Y.L. Song, S. Li, R.L. Zhang, C.M. Pan, and L. Zhang. 2010. G11R mutation in GJB6 gene causes hidrotic ectodermal dysplasia involving only hair and nails in a Chinese family. *J. Dermatol.* 37:559–561. https://doi.org/10.1111/j.1346-8138.2009.00768.x

Choi, W., N. Clemente, W. Sun, J. Du, and W. Lü. 2019. The structures and gating mechanism of human calcium homeostasis modulator 2. *Nature.* 576:163–167. https://doi.org/10.1038/s41586-019-1781-3

Contreras, J.E., J.C. Sáez, F.F. Bukauskas, and M.V. Bennett. 2003. Gating and regulation of connexin 43 (Cx43) hemichannels. *Proc. Natl. Acad. Sci. USA.* 100:11388–11393. https://doi.org/10.1073/pnas.1434298100

Darden, T., D. York, and L. Pedersen. 1993. Particle mesh Ewald: an N×log(N) method for Ewald sums in large systems. *J. Chem. Phys.* 98:10089–10092. https://doi.org/10.1063/1.464397

Demura, K., T. Kusakizako, W. Shihoya, M. Hiraizumi, K. Nomura, H. Shimada, K. Yamashita, T. Nishizawa, A. Taruno, and O. Nureki. 2020. Cryo-EM structures of calcium homeostasis modulator channels in diverse oligomeric assemblies. *Sci. Adv.* 6:eaba8105. https://doi.org/10.1126/sciadv.aba8105

Deneka, D., M. Sawicka, A.K.M. Lam, C. Paulino, and R. Dutzler. 2018. Structure of a volume-regulated anion channel of the LRRC8 family. *Nature.* 558:254–259. https://doi.org/10.1038/s41586-018-0134-y

Dreses-Werringloer, U., J.C. Lambert, V. Vingtdeux, H. Zhao, H. Vais, A. Siebert, A. Jain, J. Koppel, A. Rovelet-Lecrux, D. Hannequin, et al. 2008. A polymorphism in CALHM1 influences Ca2+ homeostasis, Abeta levels, and Alzheimer's disease risk. *Cell.* 133:1149–1161. https://doi.org/10.1016/j.cell.2008.05.048

Dumont, J.N. 1972. Oogenesis in *Xenopus laevis* (Daudin). I. Stages of oocyte development in laboratory maintained animals. *J. Morphol.* 136:153–179. https://doi.org/10.1002/jmor.1051360203

Ebihara, L. 1996. *Xenopus* connexin38 forms hemi-gap-junctional channels in the nonjunctional plasma membrane of *Xenopus* oocytes. *Biophys. J.* 71:742–748. https://doi.org/10.1016/S0006-3495(96)79273-1

Eggermont, J. 2004. Calcium-activated chloride channels: (un)known, (un) loved? *Proc. Am. Thorac. Soc.* 1:22–27. https://doi.org/10.1513/pats.2306010

Essenfelder, G.M., R. Bruzzone, J. Lamartine, A. Charollais, C. Blanchet-Bardon, M.T. Barbe, P. Meda, and G. Waksman. 2004. Connexin30 mutations responsible for hidrotic ectodermal dysplasia cause abnormal hemichannel activity. *Hum. Mol. Genet.* 13:1703–1714. https://doi.org/10.1093/hmg/ddh191

Figueroa, X.F., M.A. Lillo, P.S. Gaete, M.A. Riquelme, and J.C. Sáez. 2013. Diffusion of nitric oxide across cell membranes of the vascular wall requires specific connexin-based channels. *Neuropharmacology.* 75:471–478. https://doi.org/10.1016/j.neuropharm.2013.02.022

Gaete, P.S., and J.E. Contreras. 2020. Uncoupled permeation through large-pore channels: ions and molecules don't always ride together. *J. Physiol.* 598:209–210. https://doi.org/10.1113/JP279263

Gaete, P.S., M.A. Lillo, M. Puebla, I. Poblete, and X.F. Figueroa. 2019. CGRP signalling inhibits NO production through pannexin-1 channel activation in endothelial cells. *Sci. Rep.* 9:7932. https://doi.org/10.1038/s41598-019-44333-w

Gaitán-Peñas, H., A. Gradogna, L. Laparra-Cuervo, C. Solsona, V. Fernández-Dueñas, A. Barrallo-Gimeno, F. Ciruela, M. Lakadamyali, M. Pusch, and R. Estévez. 2016. Investigation of LRRC8-mediated volume-regulated anion currents in *Xenopus* oocytes. *Biophys. J.* 111:1429–1443. https://doi.org/10.1016/j.bpj.2016.08.030

García, I.E., J. Maripillán, O. Jara, R. Ceriani, A. Palacios-Muñoz, J. Ramachandran, P. Olivero, T. Perez-Acle, C. González, J.C. Sáez, et al. 2015. Keratitis-ichthyosis-deafness syndrome-associated Cx26 mutants produce nonfunctional gap junctions but hyperactive hemichannels when co-expressed with wild type Cx43. *J. Invest. Dermatol.* 135:1338–1347. https://doi.org/10.1038/jid.2015.20

García, I.E., F. Villanelo, G.F. Contreras, A. Pupo, B.I. Pinto, J.E. Contreras, T. Pérez-Acle, O. Alvarez, R. Latorre, A.D. Martínez, and C. González. 2018. The syndromic deafness mutation G12R impairs fast and slow gating in Cx26 hemichannels. *J. Gen. Physiol.* 150:697–711. https://doi.org/10.1085/jgp.201711782

Hansen, D.B., T.H. Braunstein, M.S. Nielsen, and N. MacAulay. 2014a. Distinct permeation profiles of the connexin 30 and 43 hemichannels. *FEBS Lett.* 588:1446–1457. https://doi.org/10.1016/j.febslet.2014.01.036

Hansen, D.B., Z.C. Ye, K. Calloe, T.H. Braunstein, J.P. Hofgaard, B.R. Ransom, M.S. Nielsen, and N. MacAulay. 2014b. Activation, permeability, and inhibition of astrocytic and neuronal large pore (hemi)channels. *J. Biol. Chem.* 289:26058–26073. https://doi.org/10.1074/jbc.M114.582155

Harris, A.L. 2007. Connexin channel permeability to cytoplasmic molecules. *Prog. Biophys. Mol. Biol.* 94:120–143. https://doi.org/10.1016/j.pbiomolbio.2007.03.011

Hartzell, C., I. Putzier, and J. Arreola. 2005. Calcium-activated chloride channels. *Annu. Rev. Physiol.* 67:719–758. https://doi.org/10.1146/annurev.physiol.67.032003.154341

Huang, N., J.F. Lian, J.H. Huo, L.Y. Liu, L. Ni, X. Yang, J.Q. Zhou, Z.F. Li, T.S. Song, and C. Huang. 2011. The EGFP/hERG fusion protein alter the electrophysiological properties of hERG channels in HEK293 cells. *Cell Biol. Int.* 35:193–199. https://doi.org/10.1042/CBI20100022

Iwao, Y., K. Yasumitsu, M. Narihira, J. Jiang, and Y. Nagahama. 1997. Changes in microtubule structures during the first cell cycle of physiologically polyspermic newt eggs. *Mol. Reprod. Dev.* 47:210–221. https://doi.org/10.1002/(SICI)1098-2795(199706)47:2<210::AID-MRD13>3.0.CO;2-3

Iwao, Y., Y. Uchida, S. Ueno, N. Yoshizaki, and Y. Masui. 2005. Midblastula transition (MBT) of the cell cycles in the yolk and pigment granule-free translucent blastomeres obtained from centrifuged *Xenopus* embryos. *Dev. Growth Differ.* 47:283–294. https://doi.org/10.1111/j.1440-169X.2005.00802.x

Jo, S., T. Kim, and W. Im. 2007. Automated builder and database of protein/membrane complexes for molecular dynamics simulations. *PLoS One.* 2:e880. https://doi.org/10.1371/journal.pone.0000880

Kanaporis, G., P.R. Brink, and V. Valiunas. 2011. Gap junction permeability: selectivity for anionic and cationic probes. *Am. J. Physiol. Cell Physiol.* 300:C600–C609. https://doi.org/10.1152/ajpcell.00316.2010

Kashio, M., G. Wei-Qi, Y. Ohsaki, M.A. Kido, and A. Taruno. 2019. CALHM1/CALHM3 channel is intrinsically sorted to the basolateral membrane of epithelial cells including taste cells. *Sci. Rep.* 9:2681. https://doi.org/10.1038/s41598-019-39593-5

Kasuya, G., T. Nakane, T. Yokoyama, Y. Jia, M. Inoue, K. Watanabe, R. Nakamura, T. Nishizawa, T. Kusakizako, A. Tsutsumi, et al. 2018. Cryo-EM structures of the human volume-regulated anion channel LRRC8. *Nat. Struct. Mol. Biol.* 25:797–804. https://doi.org/10.1038/s41594-018-0109-6

Kelm, S., J. Shi, and C.M. Deane. 2010. MEDELLER: homology-based coordinate generation for membrane proteins. *Bioinformatics.* 26:2833–2840. https://doi.org/10.1093/bioinformatics/btq554

Klauda, J.B., R.M. Venable, J.A. Freites, J.W. O'Connor, D.J. Tobias, C. Mondragon-Ramirez, I. Vorobyov, A.D. MacKerell Jr., and R.W. Pastor. 2010. Update of the CHARMM all-atom additive force field for lipids: validation on six lipid types. *J. Phys. Chem. B.* 114:7830–7843. https://doi.org/10.1021/jp101759q

Kwon, T., Q. Tang, and T.A. Bargiello. 2013. Voltage-dependent gating of the Cx32*43E1 hemichannel: conformational changes at the channel entrances. *J. Gen. Physiol.* 141:243–259. https://doi.org/10.1085/jgp.201210839

Lazic, T., K.A. Horii, G. Richard, D.I. Wasserman, and R.J. Antaya. 2008. A report of GJB2 (N14K) Connexin 26 mutation in two patients--a new subtype of KID syndrome? *Pediatr. Dermatol.* 25:535–540. https://doi.org/10.1111/j.1525-1470.2008.00767.x

Lee, E.E.L., and F. Bezanilla. 2019. Methodological improvements for fluorescence recordings in *Xenopus laevis* oocytes. *J. Gen. Physiol.* 151:264–272. https://doi.org/10.1085/jgp.201812189

Lee, J.R., A.M. Derosa, and T.W. White. 2009. Connexin mutations causing skin disease and deafness increase hemichannel activity and cell death

when expressed in *Xenopus* oocytes. *J. Invest. Dermatol.* 129:870–878. https://doi.org/10.1038/jid.2008.335

Lillo, M.A., E. Himelman, N. Shirokova, L.H. Xie, D. Fraidenraich, and J.E. Contreras. 2019. S-nitrosylation of connexin43 hemichannels elicits cardiac stress-induced arrhythmias in Duchenne muscular dystrophy mice. *JCI Insight.* 4:e130091. https://doi.org/10.1172/jci.insight.130091

Limon, A., J.M. Reyes-Ruiz, F. Eusebi, and R. Miledi. 2007. Properties of GluR3 receptors tagged with GFP at the amino or carboxyl terminus. *Proc. Natl. Acad. Sci. USA.* 104:15526–15530. https://doi.org/10.1073/pnas.0706773104

Lopez, W., J. Gonzalez, Y. Liu, A.L. Harris, and J.E. Contreras. 2013. Insights on the mechanisms of Ca$^{(2+)}$ regulation of connexin26 hemichannels revealed by human pathogenic mutations (D50N/Y). *J. Gen. Physiol.* 142:23–35. https://doi.org/10.1085/jgp.201210893

Lopez, W., J. Ramachandran, A. Alsamarah, Y. Luo, A.L. Harris, and J.E. Contreras. 2016. Mechanism of gating by calcium in connexin hemichannels. *Proc. Natl. Acad. Sci. USA.* 113:E7986–E7995. https://doi.org/10.1073/pnas.1609378113

Luo, Y., A.R. Rossi, and A.L. Harris. 2016. Computational studies of molecular permeation through connexin26 channels. *Biophys. J.* 110:584–599. https://doi.org/10.1016/j.bpj.2015.11.3528

Ma, Z., A.P. Siebert, K.H. Cheung, R.J. Lee, B. Johnson, A.S. Cohen, V. Vingtdeux, P. Marambaud, and J.K. Foskett. 2012. Calcium homeostasis modulator 1 (CALHM1) is the pore-forming subunit of an ion channel that mediates extracellular Ca^{2+} regulation of neuronal excitability. *Proc. Natl. Acad. Sci. USA.* 109:E1963–E1971. https://doi.org/10.1073/pnas.1204023109

Ma, Z., J.E. Tanis, A. Taruno, and J.K. Foskett. 2016. Calcium homeostasis modulator (CALHM) ion channels. *Pflugers Arch.* 468:395–403. https://doi.org/10.1007/s00424-015-1757-6

Maeda, S., S. Nakagawa, M. Suga, E. Yamashita, A. Oshima, Y. Fujiyoshi, and T. Tsukihara. 2009. Structure of the connexin 26 gap junction channel at 3.5 A resolution. *Nature.* 458:597–602. https://doi.org/10.1038/nature07869

Michalski, K., E. Henze, P. Nguyen, P. Lynch, and T. Kawate. 2018. The weak voltage dependence of pannexin 1 channels can be tuned by N-terminal modifications. *J. Gen. Physiol.* 150:1758–1768. https://doi.org/10.1085/jgp.201711804

Michalski, K., J.L. Syrjanen, E. Henze, J. Kumpf, H. Furukawa, and T. Kawate. 2020. The Cryo-EM structure of pannexin 1 reveals unique motifs for ion selection and inhibition. *eLife.* 9:e54670. https://doi.org/10.7554/eLife.54670

Myers, J.B., B.G. Haddad, S.E. O'Neill, D.S. Chorev, C.C. Yoshioka, C.V. Robinson, D.M. Zuckerman, and S.L. Reichow. 2018. Structure of native lens connexin 46/50 intercellular channels by cryo-EM. *Nature.* 564:372–377. https://doi.org/10.1038/s41586-018-0786-7

Nakagawa, S., X.Q. Gong, S. Maeda, Y. Dong, Y. Misumi, T. Tsukihara, and D. Bai. 2011. Asparagine 175 of connexin32 is a critical residue for docking and forming functional heterotypic gap junction channels with connexin26. *J. Biol. Chem.* 286:19672–19681. https://doi.org/10.1074/jbc.M110.204958

Nielsen, B.S., J.S. Alstrom, B.J. Nicholson, M.S. Nielsen, and N. MacAulay. 2017. Permeant-specific gating of connexin 30 hemichannels. *J. Biol. Chem.* 292:19999–20009. https://doi.org/10.1074/jbc.M117.805986

Nielsen, B.S., F. Zonta, T. Farkas, T. Litman, M.S. Nielsen, and N. MacAulay. 2019. Structural determinants underlying permeant discrimination of the Cx43 hemichannel. *J. Biol. Chem.* 294:16789–16803. https://doi.org/10.1074/jbc.RA119.007732

Nielsen, B.S., T.L. Toft-Bertelsen, S.D. Lolansen, C.L. Anderson, M.S. Nielsen, R.J. Thompson, and N. MacAulay. 2020. Pannexin 1 activation and inhibition is permeant-selective. *J. Physiol.* 598:361–379. https://doi.org/10.1113/JP278759

Orellana, J.A., E. Díaz, K.A. Schalper, A.A. Vargas, M.V. Bennett, and J.C. Sáez. 2011. Cation permeation through connexin 43 hemichannels is cooperative, competitive and saturable with parameters depending on the permeant species. *Biochem. Biophys. Res. Commun.* 409:603–609. https://doi.org/10.1016/j.bbrc.2011.05.031

Retamal, M.A., K.A. Schalper, K.F. Shoji, M.V. Bennett, and J.C. Sáez. 2007. Opening of connexin 43 hemichannels is increased by lowering intracellular redox potential. *Proc. Natl. Acad. Sci. USA.* 104:8322–8327. https://doi.org/10.1073/pnas.0702456104

Sáez, J.C., and L. Leybaert. 2014. Hunting for connexin hemichannels. *FEBS Lett.* 588:1205–1211. https://doi.org/10.1016/j.febslet.2014.03.004

Sáez, J.C., V.M. Berthoud, M.C. Brañes, A.D. Martínez, and E.C. Beyer. 2003. Plasma membrane channels formed by connexins: their regulation and functions. *Physiol. Rev.* 83:1359–1400. https://doi.org/10.1152/physrev.00007.2003

Schalper, K.A., N. Palacios-Prado, M.A. Retamal, K.F. Shoji, A.D. Martínez, and J.C. Sáez. 2008. Connexin hemichannel composition determines the FGF-1-induced membrane permeability and free [Ca$_{2+}$]$_i$ responses. *Mol. Biol. Cell.* 19:3501–3513. https://doi.org/10.1091/mbc.e07-12-1240

Schalper, K.A., H.A. Sánchez, S.C. Lee, G.A. Altenberg, M.H. Nathanson, and J.C. Sáez. 2010. Connexin 43 hemichannels mediate the Ca^{2+} influx induced by extracellular alkalinization. *Am. J. Physiol. Cell Physiol.* 299:C1504–C1515. https://doi.org/10.1152/ajpcell.00015.2010

Siebert, A.P., Z. Ma, J.D. Grevet, A. Demuro, I. Parker, and J.K. Foskett. 2013. Structural and functional similarities of calcium homeostasis modulator 1 (CALHM1) ion channel with connexins, pannexins, and innexins. *J. Biol. Chem.* 288:6140–6153. https://doi.org/10.1074/jbc.M112.409789

Smart, O.S., J.M. Goodfellow, and B.A. Wallace. 1993. The pore dimensions of gramicidin A. *Biophys. J.* 65:2455–2460. https://doi.org/10.1016/S0006-3495(93)81293-1

Syrjanen, J.L., K. Michalski, T.H. Chou, T. Grant, S. Rao, N. Simorowski, S.J. Tucker, N. Grigorieff, and H. Furukawa. 2020. Structure and assembly of calcium homeostasis modulator proteins. *Nat. Struct. Mol. Biol.* 27:150–159. https://doi.org/10.1038/s41594-019-0369-9

Tanis, J.E., Z. Ma, and J.K. Foskett. 2017. The NH$_2$ terminus regulates voltage-dependent gating of CALHM ion channels. *Am. J. Physiol. Cell Physiol.* 313:C173–C186. https://doi.org/10.1152/ajpcell.00318.2016

Taruno, A., V. Vingtdeux, M. Ohmoto, Z. Ma, G. Dvoryanchikov, A. Li, L. Adrien, H. Zhao, S. Leung, M. Abernethy, et al. 2013. CALHM1 ion channel mediates purinergic neurotransmission of sweet, bitter and umami tastes. *Nature.* 495:223–226. https://doi.org/10.1038/nature11906

Valdez Capuccino, J.M., P. Chatterjee, I.E. García, W.M. Botello-Smith, H. Zhang, A.L. Harris, Y. Luo, and J.E. Contreras. 2019. The connexin26 human mutation N14K disrupts cytosolic intersubunit interactions and promotes channel opening. *J. Gen. Physiol.* 151:328–341. https://doi.org/10.1085/jgp.201812219

van Steensel, M.A., P.M. Steijlen, R.S. Bladergroen, E.H. Hoefsloot, C.M. van Ravenswaaij-Arts, and M. van Geel. 2004. A phenotype resembling the Clouston syndrome with deafness is associated with a novel missense GJB2 mutation. *J. Invest. Dermatol.* 123:291–293. https://doi.org/10.1111/j.0022-202X.2004.23204.x

Verselis, V., R.L. White, D.C. Spray, and M.V. Bennett. 1986. Gap junctional conductance and permeability are linearly related. *Science.* 234:461–464. https://doi.org/10.1126/science.3489990

Zhang, X.J., J.J. Chen, S. Yang, Y. Cui, X.Y. Xiong, P.P. He, P.L. Dong, S.J. Xu, Y.B. Li, Q. Zhou, et al. 2003. A mutation in the connexin 30 gene in Chinese Han patients with hidrotic ectodermal dysplasia. *J. Dermatol. Sci.* 32:11–17. https://doi.org/10.1016/S0923-1811(03)00033-1
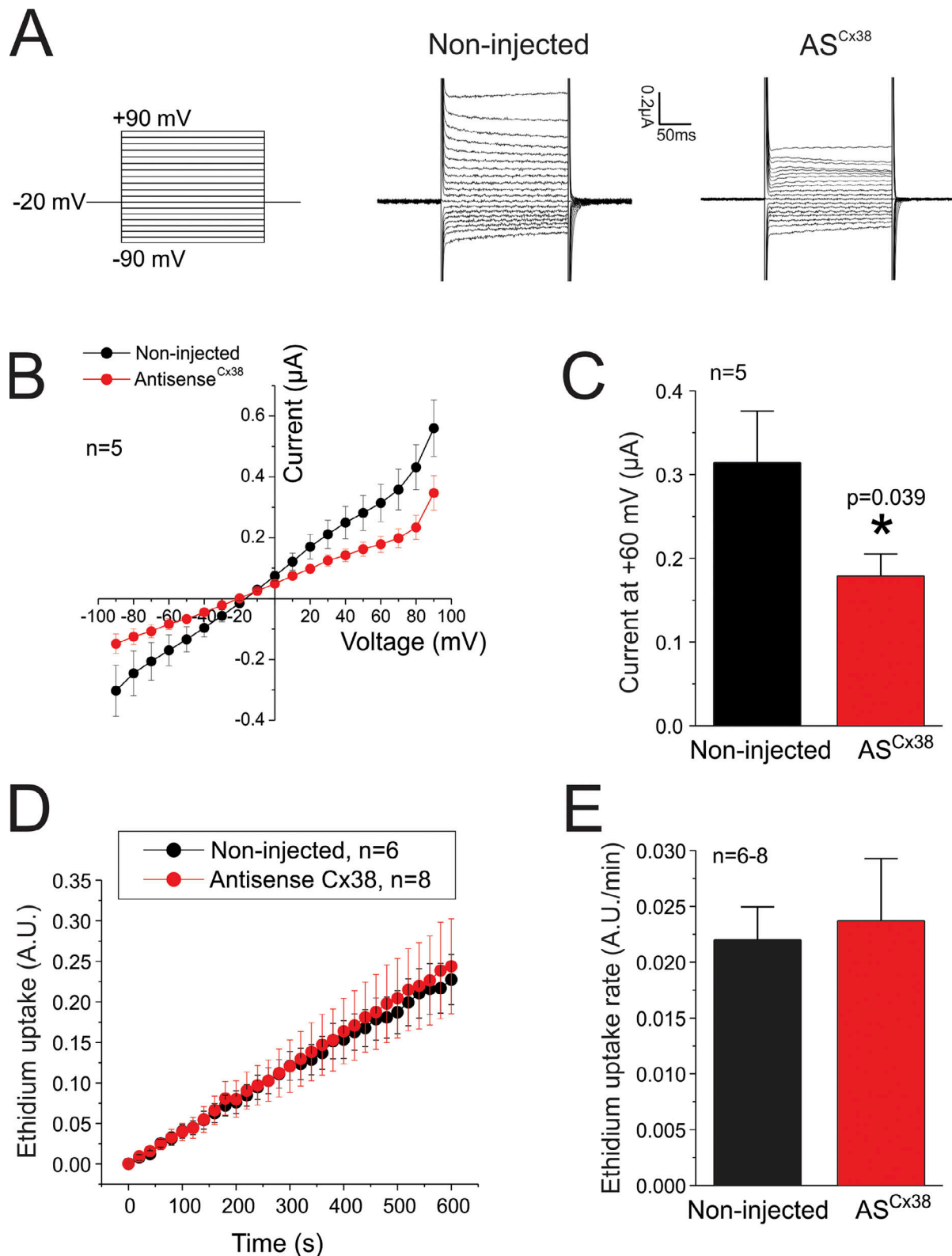
Supplemental material

Figure S1. **Effect of antisense for Cx38 on ionic currents and dye uptake. (A)** Representative traces of the ionic current observed in control noninjected oocytes or in oocytes injected with an antisense oligonucleotide to reduce the expression of endogenous Cx38 (AS[Cx38]). Currents were recorded in a divalent cation-free Ringer solution at room temperature. **(B)** I-V relationship from data shown in A. **(C)** Quantification of currents recorded at +60 mV reveals that differences are statistically significant. **(D)** Time course of the ethidium uptake recorded in noninjected oocytes and oocytes injected with AS[Cx38]. Ethidium uptake was evaluated at resting membrane potential in oocytes perfused with a divalent cation-free Ringer solution in the presence of 50 µM ethidium bromide. **(E)** Quantification of ethidium uptake rates is taken from data shown in D. All the experiments shown in this figure were performed in oocytes that did not express exogenous channels. *, $P < 0.05$ versus noninjected by unpaired Student's t test. Error bars are SEM.
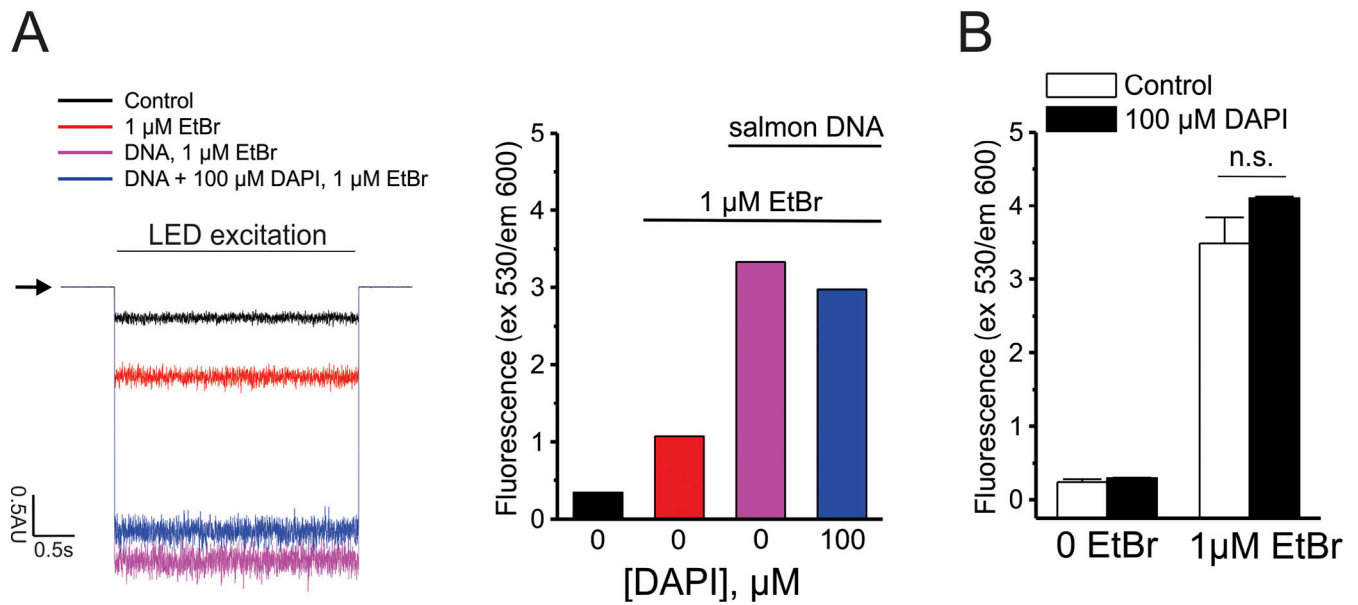
Figure S2. **DAPI does not saturate the number of binding sites available for ethidium intercalation. (A)** Left: Representative recordings of fluorescence emitted by a drop (100 µl) of water (control; black trace), 1 µM ethidium bromide (EtBr; dissolved in water; red trace), 1 µM EtBr + 0.5 mg/ml salmon DNA (magenta trace), or 1 µM EtBr + 0.5 mg/ml salmon DNA + 100 µM DAPI (blue trace). Fluorescence was detected by a photomultiplier tube in a dark room at 20–22°C. The horizontal arrow indicates the baseline where the LED is turned off. The horizontal bar indicates the period when samples are excited (3 s; excitation [ex] filter, 530 nm; emission [em] filter, 600 nm). Right: Analysis of the fluorescence shown in the left panel. **(B)** Fluorescence detected in a microplate reader in a fluorescence spectrophotometer (Cary Eclipse). Plates containing 0.5 mg/ml salmon DNA were evaluated in the absence and presence of 100 µM DAPI. Fluorescence was analyzed before (0 EtBr) and after the addition of 1 µM EtBr. n.s., nonsignificant by unpaired Student's *t* test. Error bars are SEM.
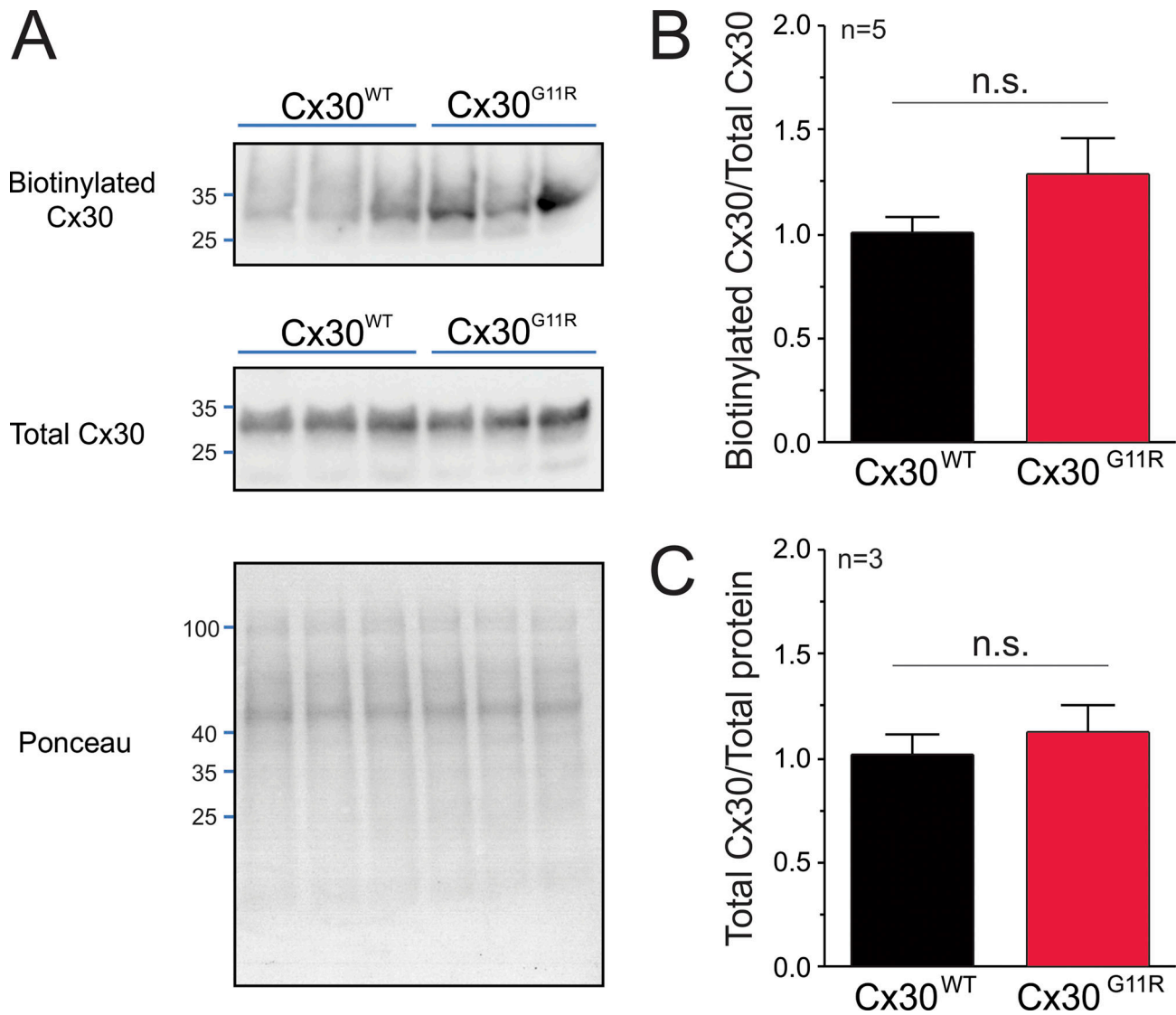
Figure S3. **The gain of function of Cx30^{G11R} channels is not associated with an increase in protein expression. (A)** Representative Western blot of biotinylated wild-type Cx30 (Cx30^{WT}) and Cx30^{G11R} expressed in *Xenopus* oocytes. In addition to the biotinylated Cx30, we examined the total Cx30. Membrane containing total protein was stained with Ponceau to show the total protein loaded in each lane. **(B)** Densitometric analysis of biotinylated Cx30. **(C)** Densitometric analysis of total Cx30. Expression of Cx30^{WT} and Cx30^{G11R} was evaluated 24 h after cRNA microinjection. In these experiments, oocytes were microinjected with the same amount of cRNA (10 ng) for Cx30^{WT} and Cx30^{G11R}. n.s., nonsignificant by unpaired Student's *t* test. Error bars are SEM.